NACA TN 3178

NATIONAL ADVISORY COMMITTEE FOR AERONAUTICS

TECHNICAL NOTE 3178

CHARACTERISTICS OF TURBULENCE IN A BOUNDARY LAYER WITH ZERO PRESSURE GRADIENT

By P. S. Klebanoff

National Bureau of Standards

Washington
July 1954

NATIONAL ADVISORY COMMITTEE FOR AERONAUTICS

TECHNICAL NOTE 3178

CHARACTERISTICS OF TURBULENCE IN A BOUNDARY LAYER WITH ZERO PRESSURE GRADIENT

By P. S. Klebanoff

SUMMARY

The results of an experimental investigation of a turbulent boundary layer with zero pressure gradient are presented. Measurements with the hot-wire anemometer were made of turbulent energy and turbulent shear stress, probability density and flattening factor of u-fluctuation (fluctuation in x-direction), spectra of turbulent energy and shear stress, and turbulent dissipation. The importance of the region near the wall and the inadequacy of the concept of local isotropy are demonstrated. Attention is given to the energy balance and the intermittent character of the outer region of the boundary layer. Also several interesting features of the spectral distribution of the turbulent motions are discussed.

INTRODUCTION

The statistical theory of turbulence introduced by Taylor and elaborated upon by Kármán, Howarth, and Dryden has played an important role in providing a sound basis for the study of turbulence. In the main, this advance has been confined to the domain of homogeneous and isotropic turbulence. At present turbulent shear flows present difficulties so formidable that statistical theories have made little progress. The older semiempirical and phenomenological theories still constitute the most tangible theoretical methods. It is now generally believed that experiment should be called upon whenever possible to furnish information on the actual behavior on the grounds that such information is needed to acquire an insight into the turbulence processes and to form the basis for a sound theoretical approach.

Experimental investigations in shear flow have made encouraging progress, largely because of the increasing number of statistical properties that may be measured by improved hot-wire techniques. Measurements have been made in the jet, wake, two-dimensional channel, pipe, and boundary layer (e.g., refs. 1 to 8). These have shown that the basic assumptions of the phenomenological theories are inconsistent

with the experimental evidence as to the nature of the turbulent motions. The work of Corrsin (ref. 1) revealed the intermittent character of turbulent flow near a free boundary. This was later studied in some detail by Townsend (ref. 2) and is now recognized as a phenomenon associated with a sharp but irregular division between turbulent and nonturbulent flow. The recent theoretical contributions of Kolmogoroff (refs. 9 and 10), Heisenberg (ref. 11), and others dealing with the concept of local isotropy and the spectrum of turbulent energy have given added impetus to experimental work in shear turbulence and have encouraged the point of view that some of the properties of isotropic turbulence may be applicable. The application of isotropy to shear flow has been rather extensively studied in wakes (ref. 3) and found to be useful, but its usefulness in a boundary layer is still questionable, especially in the region near the wall. At best, isotropy belongs to the final or dissipation stage of shear turbulence and here can throw little light on the mechanisms pertaining to shear flow. Any attempt to investigate the turbulence mechanism is hampered by the lack of an experimental technique for measurement of the pressure fluctuations. However, it is possible to obtain information pertaining to the energy balance, the study of which may be considered a proper approach to the problem. An important step in this direction in the investigation of the boundary layer was made by Townsend (ref. 6). With respect to this point of view the present work attempts to provide additional information, especially for the region close to the wall, and to obtain a more direct measure of the dissipation without relying completely on the concept of local isotropy.

Attention here is given to the boundary layer with zero pressure gradient under conditions as favorable as practicable for the use of hot-wire technique. The method of obtaining the boundary layer is described in reference 8, and the present work may be regarded as a continuation of the former work in which use is now made of an artificially thickened layer as a research tool. While there are many important features of boundary-layer turbulence, the present investigation is concerned with three major phases: The intermittency and its effects at the free boundary, energy balance, and the spectral distribution of turbulent energy and shear stress. Since the boundary layer is a complex flow combining the effects of a free boundary on the one side and those of a solid wall on the other, no one part of the layer could be deemphasized. This makes it an interesting subject if not a simple one.

The present investigation was conducted under the sponsorship and with the financial assistance of the National Advisory Committee for Aeronautics. The author wishes to express his appreciation to Dr. G. B. Shaubauer for his active support and constructive criticism and to acknowledge gratefully the assistance of Miss Z. W. Diehl and Mr. T. J. Kelly. He also wishes to thank Dr. C. M. Tchen and Dr. J. Laufer for their interest and stimulating discussions.

SYMBOLS

$$C \equiv -\left[\frac{4\delta}{5U_1^2 x_o}\int_0^{y/\delta}\frac{U}{U_1}\,d(y/\delta)\right]\frac{d}{d(y/\delta)}\left(\frac{\overline{u^2}+\overline{v^2}+\overline{w^2}}{2}\right)$$

C_f coefficient of skin friction, $\tau_o \Big/ \frac{1}{2}\rho U_1^2$

$$D \equiv \frac{\delta}{U_1^3}\frac{d}{dy}\overline{v\left(u^2+v^2+w^2+\frac{p_i}{\rho}\right)}$$

$E(k)$ three-dimensional spectral function associated with k

e voltage fluctuation

e_1 signal produced by u-component

e_2 signal produced by v-component

F flattening factor

$F_u(k_1)$ percent of turbulent energy $\overline{u^2}$ associated with k_1

$f_u(k_1)$ turbulent energy $\overline{u^2}$ associated with k_1

$f_{\overline{uv}}(k_1)$ turbulent shear stress $\overline{uv}$ associated with k_1

$f_v(k_1)$ turbulent energy $\overline{v^2}$ associated with k_1

k three-dimensional wave number

$k_s = \left(3\chi^2\epsilon/8\nu^3\right)^{1/4}$

k_1 one-dimensional wave number

n frequency

$P(u)$ probability density of u

$P(u/u')$ probability density of u/u'

$$(Pr) \equiv \frac{\delta\overline{uv}}{U_1^3}\frac{dU}{dy}$$

p	mean static pressure
p_o	mean static pressure at $x = 10.5$ feet
p_i	instantaneous pressure fluctuation
q_o	reference dynamic pressure ahead of plate
R_x	longitudinal space correlation coefficient of u-fluctuation
R_y, R_z	lateral space correlation coefficients of u-fluctuation
S	skewness factor
t	time
U	x-component of mean velocity

$$U_\tau \equiv \sqrt{\frac{\tau_o}{\rho}}$$

U_1	mean velocity in free stream
u, v, w	instantaneous turbulent velocity fluctuations in x-, y-, and z-directions, respectively
u', v', w'	root-mean-square values of u, v, and w
$\overline{u^2}$, $\overline{v^2}$, $\overline{w^2}$	mean-square values of u, v, and w
$\overline{uv}$	turbulent shearing stress
V	y-component of mean velocity

$$W_\mu \equiv \frac{\delta\nu}{U_1^3}\left(\frac{dU}{dy}\right)^2$$

$$W_1 \equiv \frac{\delta\nu}{U_1^3}\frac{d^2}{dy^2}\left(\frac{\overline{u^2} + \overline{v^2} + \overline{w^2}}{2}\right)$$

$$W_2 \equiv \frac{\delta\nu}{U_1^3}\left[\overline{\left(\frac{\partial u}{\partial x}\right)^2} + \overline{\left(\frac{\partial v}{\partial x}\right)^2} + \overline{\left(\frac{\partial w}{\partial x}\right)^2} + \overline{\left(\frac{\partial u}{\partial y}\right)^2} + \overline{\left(\frac{\partial u}{\partial z}\right)^2} + \overline{\left(\frac{\partial v}{\partial y}\right)^2} + \overline{\left(\frac{\partial v}{\partial z}\right)^2} + \overline{\left(\frac{\partial w}{\partial y}\right)^2} + \overline{\left(\frac{\partial w}{\partial z}\right)^2}\right]$$

x distance along surface from leading edge of plate

x', y', z' intervals in x-, y-, and z-directions

x_o distance along surface from virtual origin of boundary layer

y distance normal to surface measured from surface

$y^* \equiv \frac{yU_1}{\nu}$

z direction perpendicular to xy-plane

γ intermittency factor

δ boundary-layer thickness

δ_e boundary-layer energy thickness, $\int_0^\infty \frac{U}{U_1}\left[1 - \left(\frac{U}{U_1}\right)^2\right]dy$

ϵ dissipation of turbulent energy in isotropic turbulence

$\zeta = \left(\sqrt{2}\sigma/\delta\right)^{-1}\left[(y/\delta) - 0.78\right]$

θ angle between velocity vector and normal to wire

λ_x longitudinal microscale

ν kinematic viscosity

ρ density of air

σ standard deviation

τ_o shearing stress at wall

X	absolute constant
ω_x	x-component of vorticity
$\overline{( )}$	mean value

PROCEDURE AND RESULTS

Experimental Arrangement

The present investigation was conducted at the National Bureau of Standards in the $4\frac{1}{2}$-foot wind tunnel shown in figure 1. The turbulence level of the tunnel was 0.02 percent at 30 feet per second and 0.04 percent at 100 feet per second. The low level of turbulence was obtained by damping screens placed in the settling chamber. The boundary layer was developed on a smooth, flat, aluminum plate 12 feet long, $4\frac{1}{2}$ feet wide, and $\frac{1}{4}$ inch thick with a symmetrical and pointed leading edge. The plate was mounted vertically and centrally in the test section of the tunnel.

The scheme of artificially thickening of turbulent boundary layers developed in reference 8 was applied here in order to realize the advantages of a thick boundary layer, namely, the larger scales of mean and fluctuating flow fields which decrease errors due to the finite size of the hot-wire probe and the limited upper-frequency response of the equipment. In addition high Reynolds numbers are afforded without high speeds. The thickening was achieved by covering the first 2 feet of the plate with sand roughness consisting of No. 16 floor-sanding paper. At the working station $10\frac{1}{2}$ feet from the leading edge the boundary layer was 3 inches thick. All of the measurements were made at this position. The free-stream speed was 50 feet per second. The elaborate tests described in reference 8 showed that the boundary layer was the fully developed, smooth-wall type, having an apparent development length of 14.2 feet of smooth surface. The corresponding length Reynolds number based on values of x measured from the virtual origin was 4.2×10^6.

In order to obtain a condition of zero pressure gradient along the plate, the passage between the tunnel wall and the plate was made sufficiently divergent to offset the natural fall in pressure due to boundary-layer growth. This was accomplished by a flexible side wall which could be positioned by screws threaded into the tunnel wall. The final pressure distribution is shown in figure 2. From 2 feet on downstream the pressure is seen to be constant on the average with variations

about 1/2 percent of q_o about the mean. These variations were associated with the inherent waviness of the surface and could not be removed by the adjustable wall.

Instrument Mounting and Traversing

The positioning and moving of an instrument from point to point was always done in the manner that best suited the instrument and the purpose. For example, the pressure distribution along the plate was determined by means of a static tube mounted from a carriage that could be moved and positioned by remote control. Since all other types of measurements were made at the 10.5-foot station, the various measuring probes were supported on rods extending through the plate to a micrometer-screw traversing device on the opposite side. This provided adequate rigidity and negligible interference and permitted movement by known amounts to and from the surface. Initial distance from the surface was obtained by using a prism to reflect the images of the surface and the probe on the calibrated scale of a microscope.

In special cases such as the measurements of the R_y and R_z correlations, small manually operated traversing units that could be mounted to the rods were employed. In all cases adequate rigidity and freedom from interference rather than convenience of operation dictated the arrangement.

Measurement of Pressure and Mean Velocity

Nickel tubing 0.04 inch in diameter and 0.003 inch in wall thickness was used for the impact and static-pressure tubes. The static-pressure tube was made according to the conventional design for such a tube, and the pressure distribution was measured by traversing longitudinally at a distance 1/4 inch from the surface. The impact tube was flattened at the end to form a rectangular opening 0.014 inch wide and, together with a static tube similar to that used for the pressure distribution, was used to measure the mean-velocity distribution. Velocity distributions were also measured at 10 inches above and below the center line. These agreed well with the distribution at the center line and thus confirmed the two-dimensional nature of the flow. No correction was made for the effect of turbulence on the measured values nor for the effective geometric center of the impact tube.

Close to the wall, $0 < y < 0.05$ inch, the mean velocity was measured with a hot-wire. Platinum wire 0.0003 inch in diameter and approximately 1/2 inch long was used and operated at low-temperature loadings in order to minimize the influence of the wall on the heat-loss characteristics of the wire. A correction was made for the effect

of the turbulence level on the measured hot-wire values. This was done by a graphical method using the mean-velocity-voltage calibration curve and the measured root mean square of the voltage fluctuations. The corrected mean velocity was higher than the observed, with a maximum correction of about 10 percent. The hot-wire values were in good agreement with the pitot-static-tube values.

The velocity distribution is shown in figure 3. The dashed line denoting the velocity gradient at the wall was computed from the shear at the wall and is in satisfactory agreement with the measured values.

Turbulence Intensities and Shearing Stress

The hot-wire equipment used is described in detail in reference 12. The frequency response of the uncompensated amplifier was flat from 2 to 50,000 cycles and was down 17 percent at 70,000 cycles. A number of cut-off filters were provided to cut out frequencies above the range needed in a particular measurement so that unnecessary noise was eliminated. By this expedient the input noise level was held down to the order of 2 to 4 microvolts. Compensation for the time lag of the wire was determined by the square-wave method and was accomplished by a resistance-capacitance network in the amplifier. Platinum and platinum-rhodium (90 percent platinum and 10 percent rhodium) wires 0.0001 inch in diameter and 1/2 millimeter long having a time constant of approximately 0.25 millisecond were generally used. In cases where the signal-to-noise level presented some difficulty, 0.00005-inch-diameter wire was used. This was wire drawn by the Wollaston process and the method of attaching the wire was to etch away the silver and to soft-solder the wire to the supporting prongs. Fine sewing needles were used as the prongs for the u-holder and fine jeweler's broaches were used as prongs for the x-wires. No wire-length corrections were applied to any of the data. The method of measuring the turbulence intensities u', v', and w' is described in reference 13. The u', v', and w' distributions are shown in figure 4. The value of u' was obtained as close to the wall as 0.004 inch, but because of the comparatively larger size of the probes necessary for the measurement of v' and w' it was not possible to measure these closer than about 0.045 inch. The extrapolated values of v' and w' were obtained by comparing the boundary-layer values with those obtained in a pipe (ref. 5) on a basis of U_T against y^*. Good agreement existed within the measured range and consequently the pipe data which contained values corresponding to distances closer to the wall (because of the lower Reynolds number) were used as a basis for extrapolation.

The measurement of $\overline{uv}$ was made by the conventional x-wire method described in reference 13. Use was made of the experimental data for

the angle response found by Newman and Leary (ref. 14), namely, $(\cos\theta)^{0.457}$ rather than the customary $(\cos\theta)^{1/2}$ where θ is the angle between the velocity vector and the normal to the wire. The signals to be dealt with are e_1 and e_2 produced by the u- and v-components, respectively. In principle, one wire of an x-wire probe contributes the output $\overline{(e_1 + e_2)^2}$ and the other contributes $\overline{(e_1 - e_2)^2}$. The difference between these two outputs gives $\overline{e_1 e_2}$ from which $\overline{uv}$ may be calculated by employing the experimentally determined factors of proportionality.

The results are shown in figure 5. Since the viscous shearing stress reached only 2 percent of the total at the point nearest the wall, the turbulent shearing stress $\overline{uv}$ shows the characteristics of the total. It approaches the wall with zero slope as it must when the pressure gradient is zero and is in excellent agreement with the value at the wall calculated by the method of Squire and Young (ref. 15).

Spectra of $\overline{u^2}$, $\overline{v^2}$, and $\overline{uv}$

The mean-square values of the u-fluctuation between frequencies n and n + dn were obtained by feeding the signal from the compensated amplifier into a General Radio wave analyzer having a frequency range from 10 to 16,000 cps and a fixed band pass. The signal from the analyzer was then fed into a thermocouple circuit for measuring the mean-square output. In reading the output, averages were taken for a period of 1 minute. The mean-square voltage associated with the hot-wire signal passed by the band was obtained by feeding in a known sine-wave input at the proper frequency to give the same output reading. The mean-square voltage per unit frequency was then obtained by dividing by the effective band width. The effective band width had a value of 5.36 cps and was defined as the rectangular band width having the same area as the experimentally determined band shape. The results presented in figures 6 and 7 are normalized and

$$\int_0^\infty F_u(k_1)\, dk_1 = 1$$

and the wave number k_1 is given by

$$k_1 \equiv \frac{2\pi n}{U}$$

Over most of the range the accuracy was on the order of ±10 percent. The accuracy is somewhat less at the two extremes because of large-amplitude fluctuations at low frequencies and because of low signal-to-noise ratio at the high frequencies. The error due to finite length of wire increases as the scale of the turbulent motions decreases and becomes significant at the higher wave numbers. However, because of the lesser accuracy of measurement in this range no wire-length corrections were applied. The over-all value of $\overline{u^2}$ served as a check and was in good agreement with that calculated from the spectrum.

The same signals as those involved in the measurement of the over-all turbulence shear were passed through the same analyzer to obtain the spectra of $\overline{uv}$ shown in figure 8. Values below 10^{-5} should be taken with some reservation since they involve the small differences of two nearly equal signals.

The spectra of $\overline{v^2}$ shown in figures 9 and 10 were calculated from the data taken during the measurements of the shear spectra. This method, in principle, is perhaps not so accurate as a direct measurement of the v-spectra, but a check on the reliability of the measurement was afforded by comparing the u-spectra calculated from the same data with that directly measured, and in general the agreement was good.

The data for the shear and $\overline{v^2}$ spectra are not normalized so that

$$\frac{1}{U_1^2}\int_0^\infty f_{\overline{uv}}(k_1)\,dk_1 = \frac{\overline{uv}}{U_1^2}$$

and

$$\int_0^\infty f_v(k_1)\,dk_1 = \overline{v^2}$$

Probability Distribution, Skewness, and Flattening Factor of u-Fluctuations

The distribution of amplitude of u-fluctuations was determined by passing the voltage signal through a conventional gate circuit which conducted when the signal was above the level of the gate. The signal was preamplified so that the gate width could be considered negligible with respect to the root-mean-square value of the signal and the pulses

produced by the gate were a series of square waves of constant amplitude of varying duration dependent on the time the signal was above the gate. The percent of the time that the signal was above the gate with the gate set at different levels gave an integral curve from which the probability density $P(u)$ was determined by graphical differentiation where $P(u)\,du$ is defined as the fraction of the total time the fluctuation spends between u and $u + du$. A counting procedure similar to that described in reference 16 was found to offer the best means of measurement and averaging. Briefly stated, by means of a coincidence circuit the pulse from the gate permitted passage of a 100,000-cps signal for the duration of the pulse and the resultant signal was then counted by means of an electronic counter. The ratio of the number of counts to the total number of cycles during a specified time gave the desired fraction. The counting interval varied with the level of the gate and ranged from 1 minute at the 50-percent position to 5 minutes at the edge where the pulses were short and infrequent.

The midpoint was defined as the position about which the average signal was zero and is obtained from the first moment of the probability distribution, which by definition is

$$\overline{u} = \int_{-\infty}^{\infty} uP(u)\,du = 0$$

The distributions of the probability density at various positions across the boundary layer are shown in figure 11 and are expressed in values of u relative to u', so that

$$\int_{-\infty}^{\infty} P\left(\frac{u}{u'}\right) d\left(\frac{u}{u'}\right) = 1$$

At most of the positions the distributions closed in rather well and permitted the calculation with reasonable accuracy of the skewness and flattening factors, where

$$S = \frac{\int_{-\infty}^{\infty} u^3 P(u)\,du}{\left[\int_{-\infty}^{\infty} u^2 P(u)\,du\right]^{3/2}} = \frac{\overline{u^3}}{\left(\overline{u^2}\right)^{3/2}}$$

and

$$F = \frac{\int_{-\infty}^{\infty} u^4 P(u)\, du}{\left[\int_{-\infty}^{\infty} u^2 P(u)\, du\right]^2} = \frac{\overline{u^4}}{\left(\overline{u^2}\right)^2}$$

At $y/\delta = 0.8$ and $y/\delta = 1.0$ the limbs of the curves were uncertain, and no attempt was made to calculate the higher moments at these positions. The flattening factor was also measured directly. Since this involves the nondimensional ratio of the same voltage signal, that is,

$$F = \frac{\overline{e^4}}{\left(\overline{e^2}\right)^2} = \frac{\overline{u^4}}{\left(\overline{u^2}\right)^2}$$

it was not necessary to calibrate the hot-wire, but the correction for the difference in gain involved in the processing of the divided signals had to be determined by calibrating with a known sine-wave input. The fourth power was measured by feeding the signal from the compensated amplifier into an instantaneous squaring circuit, which consisted of a series of diodes properly biased to give the square of the input (ref. 12), and then squaring again with a thermocouple. The distribution of flattening factors across the boundary layer measured in this manner is given in figure 12.

It is seen from figure 11 that from $y/\delta = 0.4$ to the wall the usual safety factor of three times the root-mean-square value for determining the operating point of the equipment is quite satisfactory. In the outer region of the layer, at $y/\delta = 0.8$, this factor is exceeded in the direction of negative values of u. Here measurements were taken at varying gain-control settings to make sure that the equipment was not overloading.

Measurement of Derivatives

The usefulness of the concept of local isotropy lies in the hope that the rate of turbulent-energy dissipation in shear flow can be given in terms of the dissipation expression for isotropic turbulence. This would simplify the experimental procedure by requiring only the measurement of the mean-square derivative of the u-fluctuation with respect

to x. A fuller discussion as to the adaptability of the concept of local isotropy is given in the section entitled "Energy Balance," but it may be stated that the use of the isotropic relation in determining the dissipation is inadequate, especially in the region near the wall. It thus becomes necessary to measure all of the following nine mean-square derivatives appearing in the dissipation term of the turbulence energy equation

$$\overline{\left(\frac{\partial u}{\partial x}\right)^2} + \overline{\left(\frac{\partial v}{\partial x}\right)^2} + \overline{\left(\frac{\partial w}{\partial x}\right)^2} + \overline{\left(\frac{\partial u}{\partial y}\right)^2} + \overline{\left(\frac{\partial u}{\partial z}\right)^2} + \overline{\left(\frac{\partial v}{\partial y}\right)^2} + \overline{\left(\frac{\partial v}{\partial z}\right)^2} + \overline{\left(\frac{\partial w}{\partial y}\right)^2} + \overline{\left(\frac{\partial w}{\partial z}\right)^2}$$

In the present investigation, because of the practical limitations of hot-wire techniques it was possible to measure only the first five of the above terms. The first three were evaluated by taking the time derivative of the signal by means of a resistance-capacitance network and obtaining the mean-square value with a thermocouple and meter. The practical use of a differentiating circuit involves a compromise between attenuation and the extent of linear response with frequency. In the present measurements the differentiation was linear to 10,000 cps and was down 12 percent from linearity at 16,000 cps. This was considered adequate for the frequencies under investigation since no significant change in the measured values was obtained by varying the cut-off filters in the amplifier. The time derivative was converted to the space derivative by assuming the accuracy of the space-time transformation

$$\overline{\left(\frac{\partial u}{\partial x}\right)^2} = \frac{1}{U^2}\overline{\left(\frac{\partial u}{\partial t}\right)^2}$$

The remaining two terms were obtained by measuring the correlation coefficients R_y and R_z for a small distance of y and z and using the relations given by Taylor (ref. 17)

$$R = \frac{\overline{u(y)u(y + y')}}{u'(y)u'(y + y')} = 1 - \frac{1}{2\overline{u^2}}\overline{\left(\frac{\partial u}{\partial y}\right)^2}(y')^2$$

$$y' \longrightarrow 0$$

and

$$R_z = \frac{\overline{u(z)u(z+z')}}{\overline{u'(z)u'(z+z')}} = 1 - \frac{1}{2\overline{u^2}}\overline{\left(\frac{\partial u}{\partial z}\right)^2}(z')^2$$

$$z' \longrightarrow 0$$

The correlation coefficients were measured by the method described in reference 18 for varying distances of y' and z' ranging from 0.004 to 0.04 inch.

The distribution of the various derivatives across the boundary layer are given in figures 13 and 14.

An attempt to assess the validity of the space-time transformation was made at $y/\delta = 0.05$. In figure 15, the longitudinal correlation coefficient R_x obtained by measuring the correlation between values of u at the same instant for varying distances in the x-direction is compared with that calculated from the spectrum using the Fourier transform

$$R_x = \int_0^\infty F_u(k_1) \cos(k_1 x')\, dk_1$$

The latter gives the spatial correlation from a time correlation using the space-time relation. The microscale λ_x calculated from the spectrum is defined by

$$\frac{1}{\lambda_x^2} = \frac{1}{2}\int_0^\infty k_1^2 F_u(k_1)\, dk_1$$

It is seen that for values of x' less than 0.2 inch the two are in good agreement. They yield the same microscale, and the space-time transformation is apparently valid for the small-scale motions responsible for the dissipation. For large values of x' the two begin to diverge and the space-time relation becomes progressively worse for the larger scale motions. At $x' = 0.4$ inch the major contribution to the correlation comes from those wave numbers below 1.3 per centimeter. It seems therefore that the adequacy of the space-time transformation

depends on wave number and gives rise to the interesting speculation that the large-scale motions have their own characteristic velocities different from the mean speed. Still closer to the wall, the space-time assumption does not become a serious obstacle to the calculation of the dissipation since the magnitude is given mainly by derivatives in the y- and z-directions.

Although no wire-length corrections were applied to any of the data, it should be mentioned that an estimate of the correction was made for $\overline{\left(\frac{\partial u}{\partial y}\right)^2}$ at $y/\delta = 0.005$ by the method given in reference 19. It was approximately 10 percent and consequently wire-length corrections may be considered negligible across most of the boundary layer.

DISCUSSION

Intermittency

In shear flows that have a free boundary, it has been repeatedly observed that as the free stream is approached the turbulence becomes intermittent, that is, that for only a fraction γ of the time is the flow turbulent. This on-and-off character of the turbulence has been definitely established as being a manifestation of the irregular outline of the boundary layer as it moves downstream. The intermittency is easily observed by oscilloscope records of the u-fluctuation in the outer region of the boundary layer, and the records can be used to give a quantitative estimate of the factor γ and to discern some qualitative aspects of the flow. Representative sections of oscilloscope records taken at various positions across the boundary layer are given in figure 16. It is seen that in the outer region of the layer $y/\delta > 0.4$ there are intervals of time when the flow is not turbulent and that this time increases with increasing distance from the wall. Thus, the outer regime is divided into a turbulent part and a relatively nonturbulent free-stream part, and the hot-wire at a given position responds to alternate turbulent and nonturbulent flows as the pattern is swept downstream. A vorticity meter which responds to the vorticity that exists only in the turbulent region and suppresses the low-frequency fluctuation was used to obtain a sharper division between the turbulent and nonturbulent regions. Typical samples of the vorticity trace ω_x at different positions across the boundary layer are shown in figure 17.

The first measurements of the intermittency factor γ were those obtained by Townsend (ref. 3), where γ is taken as the ratio of the flattening factor (of u or $\partial u/dt$) in the wholly turbulent region to that in the intermittent region. From figure 12, it is seen that the

flattening factors in the region near the wall $y/\delta < 0.4$ are quite constant with a value corresponding closely to the Gaussian value of 3.0. By considering the intermittency as an on-off process the value of γ is given by

$$\gamma = 3.0 \Bigg/ \frac{\overline{u^4}}{\left(\overline{u^2}\right)^2}$$

The intermittencies calculated in this manner together with those calculated from the oscilloscope records of the u-fluctuation and the vorticity are given in figure 18. Values of γ obtained from the flattening factor are consistent with those obtained from the film only up to $y/\delta = 0.9$. As seen in figure 12, the flattening factors reach a maximum and then begin to decrease. This is not too surprising because for low values of γ the turbulence of the free stream would be expected to make itself felt. The result is probably a weighting of the probability density for the turbulence of the free stream with that within the boundary, which depends on the relative turbulence levels and the degree of intermittency. The curve in figure 18, which closely represents the variation of γ with y/δ, is a Gaussian integral curve given by

$$\gamma = \frac{1}{2}(1 - \operatorname{erf} \zeta)$$

where

$$\zeta = \left(\sqrt{2}\,\frac{\sigma}{\delta}\right)^{-1}\left[\left(\frac{y}{\delta}\right) - 0.78\right]$$

and

$$\left(\sqrt{2}\,\frac{\sigma}{\delta}\right)^{-1} = 5$$

The standard deviation σ is

$$\sigma = 0.14\delta$$

Such a distribution indicates that the instantaneous position of the edge of the boundary layer has a random character with a mean position at $y/\delta = 0.78$. The edge rarely extends outside the region $y/\delta = 0.4$ to 1.2. While the position of the edge fluctuates over a large fraction of δ, the mean velocity is near that of the free stream, being down by at most about 15 percent.

Several interesting features can be gleaned from careful study of the oscilloscope records. Although it may be difficult to see from the short sections given in figure 16, it was noticed that in the strongly intermittent region, for example at $y/\delta = 0.8$, the trace had somewhat of a square-wave appearance. Increasing velocities are in the direction of the timing signal. The nonturbulent regions seem to be at a constant level corresponding to that of the free stream, while the turbulence regions are seen to be centered about some lower level. The difference between the velocity of the outside potential flow and that existing in the turbulent region seemed to depend on how far past the measuring position the instantaneous edge of the layer extended at the particular instant. At $y/\delta = 1.0$ and 1.2 there is very little evidence of the shift because the edge does not extend to any great distance beyond these positions. There is then a step as well as the on-off process which was assumed in the calculation of γ from the flattening factor. The agreement with values obtained from the film is probably due to the lack of sensitivity of the flattening factor to this shift. However, the skewness factor can be expected to be extremely sensitive.

A sketch of the boundary layer is given in figure 19. The boundary between the turbulent flow and the free stream is quite sharp, and the properties of the shear layer are comparatively distinct from those in the free stream. The boundary layer travels downstream with an outline constantly changing in an irregular manner, and the intermittency is characterized by a large-scale diffusion process, carrying with it small-scale turbulent motions. From the film taken at $y/\delta = 0.8$ it was also noticed that the average frequency of the occurrence of periods of no turbulence seemed to be approximately 100 per second, and, since the pattern is moving with nearly the free-stream speed of 50 feet per second, a rough estimate of the average wave length for the irregular outline of the boundary layer would appear to be approximately 2δ or 14σ.

The effect of the intermittency on the probability density is clearly seen from figure 11. In the nonintermittent region the distributions are very nearly Gaussian and the values of skewness and flattening factor calculated from the measured probabilities are given in the following table:

y/δ	F	S
0.001	2.52	0.09
.05	2.75	-.08
.2	2.62	-.08
.4	3.19	-.26

Calculations of the higher moments of the probability densities from the distributions tend to be inaccurate because of their emphasis on the higher values of u. However, the values of flattening factor agree fairly well with the directly measured values. Values of skewness should be taken with some reservation because they are extremely sensitive to the accuracy of the midpoint. Also in the region near the wall where turbulent fluctuations are large the nonlinear response of the hot-wire tends to skew the signal. At $y/\delta = 0.8$ the probability density is very strongly negatively skewed because of the lower velocities within the turbulent regions. At the same time the large percent of time that the nonturbulent regions exist causes the maximum to be displaced to the positive side of the midpoint. The distribution at $y/\delta = 1.0$ has a flattening in qualitative agreement with the trend of the flattening factor to reach a maximum and then to decrease. The distributions of skewness show the same general trend. The maximum of the probability distribution for $y/\delta = 1.0$ is displaced slightly to the left of $u = 0$, and it is uncertain whether this is experimental or a consequence of the weighting effect previously mentioned in connection with the flattening factor.

By assuming that the free-stream regions contribute little to the measured mean-turbulence quantities, an allowance may be made for the effect of intermittency by dividing by the factor γ. The distributions of turbulent energy and shear stress divided by γ are given in figure 20. The distribution of turbulent energy within the bounded flow is strikingly similar to that for channel and pipe flow (refs. 4 and 5) as is the distribution of turbulent shear stress which is approximately linear from $y/\delta = 0.1$ to $y/\delta = 1.0$.

Intermittency is, of course, absent from fully developed turbulent flow in pipes and channels because there is no free stream. It is well-known that the mean velocity for pipe and channel does not deviate as much from the logarithmic distribution as does that of the boundary layer, and a major factor in this discrepancy is the intermittency. The influence of intermittency on the mean-velocity distribution is difficult to ascertain, being in the nature of a complex time-averaging problem. Although something may be done in a semiempirical fashion by introducing γ into the mixing-length theories, it contributes little to the basic understanding of the problem. Since the turbulent stress is apparently confined only to the turbulent portions of the flow, there arises the question as to the actual mean-velocity gradients in which the shear stress exists. In figure 21 the measured mean velocity is plotted in the form suggested by the velocity-defect law, and it is seen that the characteristic logarithmic law exists only in a limited range from about $y/\delta = 0.01$ to $y/\delta = 0.2$. The direct viscous dissipation (fig. 22) is negligible at $y/\delta = 0.01$. This corresponds to a value of $y^* = 27.6$, which is in good agreement with the usually observed value of 30 for pipe and channel. An interesting point to note is that in the range of

$y/\delta = 0.1$ to $y/\delta = 0.8$ the ratio of shear stress to turbulent energy is approximately constant, as is also evidenced by the constancy of the shear correlation coefficient in figure 5. This would tend to indicate some degree of "Kármán similarity" existing in the range where the distribution deviates from the logarithmic law. In addition Kármán similarity requires that the large-scale motions responsible for the shear stress be free from the effects of viscosity, which, as will be seen in the section on spectra, is much more justified in the region where the logarithmic law is not obeyed than in the region where it is obeyed. Although any correction for the effect of intermittency is in the direction of minimizing this deviation, it is pointed out that the mean-velocity distributions for pipe and channel also deviate in this region. It is difficult to attach any particular significance to the logarithmic law which exists for so limited a range of the boundary layer, except that it is a region where the direct influence of the wall may still be present. It is not apparent that a degree of validity can be assigned to it on the basis of the various forms of the mixing-length theory. With respect to the mean velocity, the boundary layer can be divided into three regions, namely, a viscous region extending to a value of $y^* = 30$, an intermediate region where the influence of the wall still exists, and an outer region characterized by intermittency.

Energy Balance

After the usual boundary-layer approximations are made, the equation expressing the energy balance for the turbulence at a given cross section in a two-dimensional boundary layer is given by

$$\overline{uv}\frac{\partial U}{\partial y} + \frac{1}{2}\frac{\partial}{\partial y}\left(\overline{u^2v} + \overline{v^3} + \overline{vw^2}\right) + \frac{1}{\rho}\frac{\partial}{\partial y}(\overline{p_i v}) + \frac{1}{2}U\frac{\partial}{\partial x}\left(\overline{u^2} + \overline{v^2} + \overline{w^2}\right) +$$

$$\frac{1}{2}V\frac{\partial}{\partial y}\left(\overline{u^2} + \overline{v^2} + \overline{w^2}\right) - \nu\left(\overline{u\nabla^2 u} + \overline{v\nabla^2 v} + \overline{w\nabla^2 w}\right) = 0$$

The respective terms from left to right have the following physical interpretation:

(1) Production of turbulent energy from the mean motion
(2) Turbulent energy diffusion
(3) Pressure diffusion
(4) Convection of turbulent energy by the x-component of the mean motion

(5) Convection of turbulent energy by the y-component of the mean motion

(6) Dissipation of turbulent energy

The convection of turbulent energy is negligible near the wall and is significant only in the outer region of the layer where similarity on the scale of δ has been experimentally observed. Consequently, by using the continuity relations

$$\frac{\partial U}{\partial x} + \frac{\partial V}{\partial y} = 0$$

and

$$\delta \propto x_o^{4/5}$$

the convection terms can be transformed into the single term which may be written in the nondimensional form

$$-\left[\frac{4}{5}\frac{\delta}{U_1^2 x_o}\int_0^{y/\delta}\frac{U}{U_1}\,d(y/\delta)\right]\frac{d}{d(y/\delta)}\left(\frac{\overline{u^2}+\overline{v^2}+\overline{w^2}}{2}\right)$$

where x_o is the distance from the virtual origin of the boundary layer. The dissipation term is not in a form that lends itself to measurement by hot-wire techniques. However, it can be rewritten in the following more suitable form:

$$\nu\frac{d^2}{dy^2}\left(\frac{\overline{u^2}+\overline{v^2}+\overline{w^2}}{2}\right) - \nu\left[\overline{\left(\frac{\partial u}{\partial x}\right)^2} + \overline{\left(\frac{\partial v}{\partial x}\right)^2} + \overline{\left(\frac{\partial w}{\partial x}\right)^2} + \overline{\left(\frac{\partial u}{\partial y}\right)^2} + \overline{\left(\frac{\partial u}{\partial z}\right)^2} + \overline{\left(\frac{\partial v}{\partial y}\right)^2} + \overline{\left(\frac{\partial v}{\partial z}\right)^2} + \overline{\left(\frac{\partial w}{\partial y}\right)^2} + \overline{\left(\frac{\partial w}{\partial z}\right)^2}\right]$$

All of the pertinent terms in the energy balance can be calculated from the measurements previously discussed except the diffusion terms which are treated as one and obtained by balancing the equation. The distributions of the various energy terms are given in figures 23, 24, and 25 in nondimensional form using δ and U_1. The turbulent shear stress in the region $0 < y/\delta < 0.05$ was obtained by subtracting the

viscous shear stress (calculated from the mean-velocity gradient) from the constant value of total shear stress as given by the shear at the wall. The second derivative term is important only in the region near the wall. Its calculation is quite uncertain and is given mainly to show its order of magnitude. The finite intercept at the wall is a consequence of the arbitrary linear extrapolation of the turbulence intensity to zero. The dissipation term is the most difficult to determine because of the importance of the region near the wall. The application of the concept of local isotropy is strongly conditioned by the local similarity of the eddies responsible for the dissipation, the verification of which is dependent on the dissipation derivatives obeying the isotropic relation

$$\overline{\left(\frac{\partial u}{\partial x}\right)^2} = \frac{1}{2}\overline{\left(\frac{\partial v}{\partial x}\right)^2} = \frac{1}{2}\overline{\left(\frac{\partial w}{\partial x}\right)^2} = \cdots$$

From figures 13 and 14 it is seen that only in the outer region of the boundary layer, $y/\delta > 0.7$, is this condition satisfied and that the derivatives become increasingly divergent as the wall is approached. The terms $\overline{\left(\frac{\partial u}{\partial y}\right)^2}$ and $\overline{\left(\frac{\partial u}{\partial z}\right)^2}$ are equal across the layer, and at $y/\delta = 0.005$ their ratio to $\overline{\left(\frac{\partial u}{\partial x}\right)^2}$ is 10 times that given by isotropy. This illustrates the very small scale nature of the turbulent motions in the transverse directions as compared with the longitudinal in the region close to the wall. The inadequacy of local isotropy is strikingly seen from the over-all energy balance obtained by integrating the energy equation across the boundary layer. The integrals of the diffusion terms and the second-derivative term are each zero, and the total production is balanced by the total dissipation plus the total convection. Using the isotropic relation $15\nu\overline{\left(\frac{\partial u}{\partial x}\right)^2}$ for the rate of dissipation of turbulent energy, the result is out of balance, with the dissipation being too low by a factor of 2.1. Hence, in order to obtain an accurate measure of the dissipation, it is necessary to measure all nine derivatives. Since it was possible to measure only the first five,

the remaining four were obtained by the arbitrary assumption that derivatives with respect to y and z are given by the isotropic relations

$$\overline{\left(\frac{\partial u}{\partial y}\right)^2} = 2\overline{\left(\frac{\partial v}{\partial y}\right)^2} = \overline{\left(\frac{\partial w}{\partial y}\right)^2}$$

$$\overline{\left(\frac{\partial u}{\partial z}\right)^2} = \overline{\left(\frac{\partial v}{\partial z}\right)^2} = 2\overline{\left(\frac{\partial w}{\partial z}\right)^2}$$

This considerably improved the total energy balance. As seen from figure 23, the dissipation calculated in this manner was obtained as close to the wall as $y/\delta = 0.005$, and if it is assumed in order to close in the dissipation curve that the dissipation is equal to the production in the region $0 < y/\delta < 0.01$, the disparity is 15 percent. This can represent a significant difference in the point-to-point balance as manifested by the diffusion term. When the diffusion term is compared with that obtained by Townsend (ref. 6), the same general trend is observed although there is a considerable difference in magnitude. The necessary balance cannot be achieved by the gain in energy due to diffusion in the region $y/\delta > 0.6$ unless it is extrapolated to an unreasonably long distance. Consequently the conclusion is that the turbulent-energy dissipation is greater than the production in a very thin region next to the wall in order to provide the dissipation needed. This means a diffusion of energy toward the wall. Townsend's values for the kinetic-energy-diffusion term require a movement of kinetic energy away from the wall. Therefore, if energy goes toward the wall it must be due to the action of pressure forces (pressure diffusion). This intense dissipative region for the turbulence apparently coincides with the viscous region for the mean flow. The magnitude of the diffusion term illustrates the weakness of the mixing-length theory which has the implicit assumption that what is locally produced is locally dissipated.

This flow of energy against the energy gradient is rather surprising and contrary to what is intuitively expected. It does not seem possible that such a result could be brought about incorrectly by the questionable assumption made regarding those dissipation derivatives that could not be measured. Neither does it seem reasonable that these derivatives can be distributed in such a manner as to make the production equal to the dissipation at all points across the layer. However, it is felt that the situation is complicated by the phenomenon of intermittency. The energy-balance equation as used does not include the effect of intermittency, in particular its effect on the production term. Perhaps the results should be accepted as tentative until a fuller understanding of the role played by the intermittency is available.

The energy balance for the mean motion is conveniently expressed in terms of the energy thickness δ_e such that

$$\frac{2\delta}{U_1^3}\int_0^1\left[\overline{uv}\,\frac{dU}{dy}+\nu\left(\frac{dU}{dy}\right)^2\right]d(y/\delta)=\frac{d\delta_e}{dx} \tag{1}$$

where

$$\delta_e=\delta\int_0^1\frac{U}{U_1}\left[1-\left(\frac{U}{U_1}\right)^2\right]d(y/\delta)$$

Similarity of the mean-velocity distribution permits treating the integral in the expression for δ_e as a constant. If δ is given by

$$\delta=0.37\nu^{1/5}U_1^{-1/5}x_o^{4/5}$$

then

$$\frac{d\delta_e}{dx}=0.296\nu^{1/5}U_1^{-1/5}x_o^{-1/5}\int_0^1\frac{U}{U_1}\left[1-\left(\frac{U}{U_1}\right)^2\right]d(y/\delta)$$

Equation (1) states that part of the loss of kinetic energy of the mean motion goes directly into heat through the action of viscosity and the remainder goes into the production of turbulent energy. The energy balance was found to be satisfied to within a few percent and served as a welcome check on the accuracy of the measurements. The production of turbulent energy and the viscous dissipation are compared for the region near the wall in figure 22. This emphasizes the importance of the region near the wall. In fact, almost 40 percent of the loss in kinetic energy of the motion is directly dissipated by viscosity in the region $0 < y^* < 30$, and of the remaining 60 percent which is converted into turbulent energy 30 percent is produced in the same region. Thus, if the conclusion drawn from the turbulent-energy balance is correct, 85 percent of the total dissipation (viscous and turbulent) takes place in $y^* < 30$.

Energy and Shear-Stress Spectra

It is possible to gain some further insight into shear flow by examining the spectral distributions of turbulent energy and shear stress. A significant advance in dealing with the energy spectrum has been made in the domain of homogeneous and isotropic turbulence (refs. 9 and 10). The basic concept underlying this advance is that energy enters the spectrum through the large eddies and is then transferred through the spectrum to the smaller eddies where it is finally dissipated. If the lower wave numbers are excluded there exists a range in which the eddies are in a state of equilibrium, governed by the rate at which they transfer and dissipate energy. When the Reynolds number is high enough, inertial forces will predominate in the lower wave numbers of this equilibrium range, and a relatively pure transfer region will exist. By dimensional reasoning it can be shown that the spectrum will vary as $k^{-5/3}$ in this range. Heisenberg (ref. 11) extended this concept by assuming that the transfer of energy at wave number k was caused by a turbulence friction produced by eddies with wave number greater than k. He represented the energy balance in the equilibrium range for homogeneous and isotropic turbulence as

$$\epsilon = \left[\nu + \chi \int_k^\infty \sqrt{\frac{E(k'')}{(k'')^3}}\, dk''\right] \int_0^k 2(k')^2 E(k')\, dk' \tag{2}$$

The second term within the brackets represents a turbulent viscosity and χ is an absolute constant. The solution of this equation gives the spectrum in the following form

$$E(k) = \left(\frac{8\epsilon}{9\chi}\right)^{2/3} k^{-5/3} \left[1 + \left(\frac{k}{k_s}\right)^4\right]^{-4/3} \tag{3}$$

where k_s is a wave number in the intermediate range given by

$$k_s = \left(\frac{3\chi^2\epsilon}{8\nu^3}\right)^{1/4}$$

For low wave numbers $E(k)$ varies as $k^{-5/3}$, and for the high-wave-number end where viscous forces predominate, as k^{-7}.

Although equation (2) involves an assumed mechanism that may not entirely represent the facts, it seems to be a reasonably good approximation. Where the Reynolds number is sufficiently high, there is

evidence of a $k^{-5/3}$ range and a transition to higher negative powers approaching -7 as k increases. There is some doubt as to whether -7 is the correct value in the limit. The concept embodied in equation (2) provides a rational basis for an approach to the problem of shear turbulence. However, the extension to shear flow is complicated by the presence of such factors as production, diffusion, convection, and the absence of isotropy and homogeneity. Any conclusions as to the effects of the diffusion and convection are difficult to draw. It may be assumed that such effects are confined to the very low wave numbers which lie outside the equilibrium range. In addition, the convection may be considered negligible across most of the layer. An attempt to assess the influence of the production term in the equilibrium range of the spectrum was made by Tchen (ref. 20). By considering the influence of the mean-velocity gradient the conclusion is reached that a range of k^{-1} will exist in the wave-number region where $k^{-5/3}$ normally exists when there is no gradient.

An experimental test of theoretical predictions is rendered difficult by the fact that only the one-dimensional spectrum can be measured. In isotropic turbulence this is not too restrictive a factor because the transformation from the three-dimensional spectral function such as appears in equation (3) to the one-dimensional spectral function is known (ref. 11). In shear flow this relation is not known, and one has to be content with the qualitative inference that in some unknown manner the one-dimensional spectrum is still an integral effect of the three-dimensional. Despite the aforementioned complications the measured spectra are of interest, and several interesting features can be noted.

The spectra of $\overline{u^2}$ at various cross-sectional positions are given in figures 6 and 7. The trend, in going toward the surface, is for the higher wave numbers to have a greater percentage of the turbulent energy. This is in accord with the trend of the shear-stress spectra (fig. 8) also to extend to higher and higher wave numbers as the wall is approached. It is noted that nearly all of the turbulent energy lies within the stress-producing range. The spectrum of shear stress at $y/\delta = 0.2$ shows an increase over that at $y/\delta = 0.05$ in the lower wave numbers. This may be indicative of the influence of the wall becoming negligible at $y/\delta = 0.2$. For $y/\delta > 0.2$ the decrease in shear stress across the boundary layer takes place for the entire spectral range. All of the energy spectra indicate the existence of a region varying as k_1^{-7} at the high-number end, but because of the lesser accuracy of the measurements in this range no direct comparison has been made. In the outer region of the layer at $y/\delta = 0.58$ and 0.8 there is an extensive region where the spectrum of $\overline{u^2}$ varies as $k_1^{-5/3}$ corresponding to the inertial subrange. The effect of intermittency in this region is difficult to ascertain except to say that it may be confined to the

low-wave-number end of the spectrum. Also the maximum in the spectrum at $y/\delta = 1.0$ is apparently a consequence of intermittency. There is a gradual transition in the shape of the spectrum from $y/\delta = 0.58$ to $y/\delta = 0.05$ where there is a wave-number range with the slope k_1^{-1} as predicted by Tchen. The small-scale nature of the turbulence near the wall is shown by the spectrum of $\overline{u^2}$ at $y/\delta = 0.0011$. The dip in the spectrum at the low-wave-number end as indicated by the dashed curve may be due to experimental error. However, it was repeatable and attention is drawn to it because it may be a result of some characteristic phenomenon associated with the laminar sublayer.

Empirically the isotropic relation for the dissipation is in fair agreement with that given in figure 24 from $y/\delta = 0.05$ to 1.0. By assuming that the second moments of the spectra (fig. 26) are a fair representation of the total dissipation, it is seen that in going toward the wall the shear penetrates deeper and deeper into the dissipation spectrum. For example, at $y/\delta = 0.58$ the wave-number range up to where $\frac{1}{U_1^2} f_{\overline{uv}}(k_1)$ has fallen to 10^{-5} contains approximately 10 percent of the dissipation. At $y/\delta = 0.05$ this figure is 30 percent. It is reasonable to expect this trend to continue, with the result that very close to the wall the turbulence produced is directly dissipated and there is no significant transfer of energy along the spectrum. This conclusion is consistent with the small-scale turbulence near the wall, and the rapidly decreasing spectrum at $y/\delta = 0.0011$.

The shear spectrum is a direct test of local isotropy, and it is evident that the range of wave numbers for which local isotropy exists becomes progressively smaller as the wall is approached. The transfer range, as evidenced by $k_1^{-5/3}$, has not yet become locally isotropic since the shear spectra approach zero at some higher wave number. However, the energy spectrum is apparently insensitive to the small amount of shear stress which does exist. In figures 9 and 10 the measured spectra of $\overline{v^2}$ at $y/\delta = 0.05$ and 0.58 are compared with those calculated from the measured $\overline{u^2}$ spectra using the isotropic relation

$$f_v(k_1) = \frac{f_u(k_1)}{2} - \frac{k_1}{2} \frac{d}{dk_1} f_u(k_1)$$

which, strictly speaking, is valid only for the range of local isotropy. It is seen that the measured $\overline{v^2}$ spectra agree with the calculated at the higher wave numbers. This is consistent with the range of local

isotropy indicated by the spectra of shear, and the difference between the over-all $\overline{u^2}$ and $\overline{v^2}$ is confined to the lower wave numbers.

From the turbulent-energy equations for the individual velocity components it is seen that the terms responsible for the exchange of energy among the various components are the pressure terms $\overline{p_i \frac{\partial u}{\partial x}}$, $\overline{p_i \frac{\partial v}{\partial y}}$, and $\overline{p_i \frac{\partial w}{\partial z}}$. The spectral range of such transfer is unknown but a reasonable speculation would be that the pressure term $\overline{p_i \frac{\partial v}{\partial y}}$ responsible for the transfer of energy to $\overline{v^2}$ exists in the same wave-number range as the shear-stress spectra. There is little evidence in the measured $\overline{v^2}$ spectrum of a range of $k_1^{-5/3}$ as observed for the spectrum of $\overline{u^2}$. This may be a consequence of the spectral distribution of the pressure term being different from that of the shear stress with a weighting more to the higher wave number end of this range.

CONCLUSIONS

The following conclusions were obtained from an investigation of characteristics of turbulence in a boundary layer with zero pressure gradient. Here y is the distance normal to the surface measured from the surface, y^* is y times the square root of the shearing stress at the wall divided by the density of air over the kinematic viscosity $(yU_\tau/\nu$ where $U_\tau \equiv \sqrt{\tau_o/\rho})$, and δ is the boundary-layer thickness.

1. The turbulent boundary layer can be considered to be divided into three regions: A viscous region extending beyond the laminar sublayer to a value of $y^* = 30$, an intermediate region from $y^* = 30$ to approximately $y/\delta = 0.2$ where the influence of the wall still exists, and an outer region characterized by the phenomenon of intermittency.

2. The turbulent boundary layer has a sharp outline constantly changing in an irregular manner. The turbulent regions travel with a velocity lower than that of the free stream. A rough estimate of the average wave length of this irregular boundary would be approximately 2δ.

3. The position of the edge of the layer with respect to the surface is approximated closely by a Gaussian distribution centered at 0.78δ with a standard deviation equal to 0.14δ.

4. The probability density of the u-fluctuation is very close to Gaussian in the region $y/\delta < 0.4$.

5. The importance of the region near the wall has been demonstrated; in fact, approximately 85 percent of the total dissipation (viscous and turbulent) takes place within $y^* < 30$. The production of turbulent energy and the turbulent-energy dissipation reach a sharp maximum within this region, and there is an inward flow of energy toward the wall because of the action of pressure forces.

6. The concept of local isotropy is inadequate for obtaining the turbulent-energy dissipation, especially in the region near the wall.

7. In the outer region of the boundary layer where the mean-velocity gradient is small the existing theories for the energy spectrum in isotropic turbulence can be applied. As the wall is approached the nonisotropy becomes significant with a resultant change in the spectrum. Very close to the wall, the turbulent energy produced is directly dissipated with no significant transfer of energy through the spectrum.

8. As close to the wall as $y/\delta = 0.05$ it has been shown that the space-time transformation is valid for the smaller eddies responsible for the turbulent dissipation but becomes invalid for the larger eddies.

National Bureau of Standards,
Washington, D. C., May 8, 1953.

REFERENCES

1. Corrsin, Stanley: Investigation of Flow in an Axially Symmetrical Heated Jet of Air. NACA WR W-94, 1943. (Formerly NACA ACR 3L23.)

2. Townsend, A. A.: The Fully Developed Turbulent Wake of a Circular Cylinder. Australian Jour. Sci. Res., ser. A, vol. 2, no. 4, 1949, pp. 451-468.

3. Townsend, A. A.: Local Isotropy in the Turbulent Wake of a Cylinder. Australian Jour. Sci. Res., ser. A, vol. 1, no. 2, 1948, pp. 161-174.

4. Laufer, John: Investigation of Turbulent Flow in a Two-Dimensional Channel. NACA Rep. 1053, 1951. (Supersedes NACA TN 2123.)

5. Laufer, John: The Structure of Turbulence in Fully Developed Pipe Flow. NACA TN 2954, 1953.

6. Townsend, A. A.: The Structure of the Turbulent Boundary Layer. Proc. Cambridge Phil. Soc., vol. 47, pt. 2, Apr. 1951, pp. 375-395.

7. Schubauer, G. B., and Klebanoff, P. S.: Investigation of Separation of the Turbulent Boundary Layer. NACA Rep. 1030, 1951. (Supersedes NACA TN 2133.)

8. Klebanoff, P. S., and Diehl, Z. W.: Some Features of Artificially Thickened Fully Developed Turbulent Boundary Layers With Zero Pressure Gradient. NACA Rep. 1110, 1952. (Supersedes NACA TN 2475.)

9. Kolmogoroff, A. N.: The Local Structure of Turbulence in Incompressible Fluid for Very Large Reynolds' Numbers. Comp. rend., Acad. Sci. URSS, vol. 30, no. 4, Feb. 10, 1941, pp. 301-305.

10. Kolmogoroff, A. N.: Dissipation of Energy in the Locally Isotropic Turbulence. Comp. rend., Acad. Sci. URSS, vol. 32, no. 1, July 10, 1941, pp. 16-18.

11. Heisenberg, W.: Zur statistischen Theorie der Turbulenz. Zs. Phys., Bd. 124, Heft 7/12, 1948, pp. 628-657.

12. Kovásznay, Leslie S. G.: Development of Turbulence Measuring Equipment. NACA Rep. , 1954. (Supersedes NACA TN 2839.)

13. Schubauer, G. B., and Klebanoff, P. S.: Theory and Application of Hot-Wire Instruments in the Investigation of Turbulent Boundary Layers. NACA WR W-86, 1946. (Formerly NACA ACR 5K27.)

14. Newman, B. G., and Leary, B. G.: The Measurement of the Reynolds Stresses in a Circular Pipe as a Means of Testing a Hot Wire Anemometer. Rep. A.72, Dept. of Supply, Aero. Res. Lab., Australia, Nov. 1950.

15. Squire, H. B., and Young, A. D.: The Calculation of the Profile Drag of Aerofoils. R. & M. No. 1838, British A.R.C., 1938.

16. Leipmann, H. W., and Robinson, M. S.: Counting Methods and Equipment for Mean-Value Measurements in Turbulence Research. NACA TN 3037, 1953.

17. Taylor, G. I.: Statistical Theory of Turbulence III - Distribution of Dissipation of Energy in a Pipe Over Its Cross-Section. Proc. Roy. Soc. (London), ser. A, vol. 151, no. 873, Sept. 2, 1935, pp. 455-464.

18. Dryden, Hugh L., Schubauer, G. B., Mock, W. C., Jr., and Skramstad, H. K.: Measurements of Intensity and Scale of Wind-Tunnel Turbulence and Their Relation to the Critical Reynolds Number of Spheres. NACA Rep. 581, 1937.

19. Uberoi, Mahinder S., and Kovásznay, Leslie S. G.: Influence of Resolving Power on Measurement of Correlations and Spectra of Random Fields. Tech. Rep. No. 30, Project Squid, Johns Hopkins Univ., 1952.

20. Tchen, C. M.: On the Spectrum of Energy in Turbulent Shear Flow. Res. Paper RP2388, Jour. Res., Nat. Bur. Standards, vol. 50, no. 1, Jan. 1953, pp. 51-62.

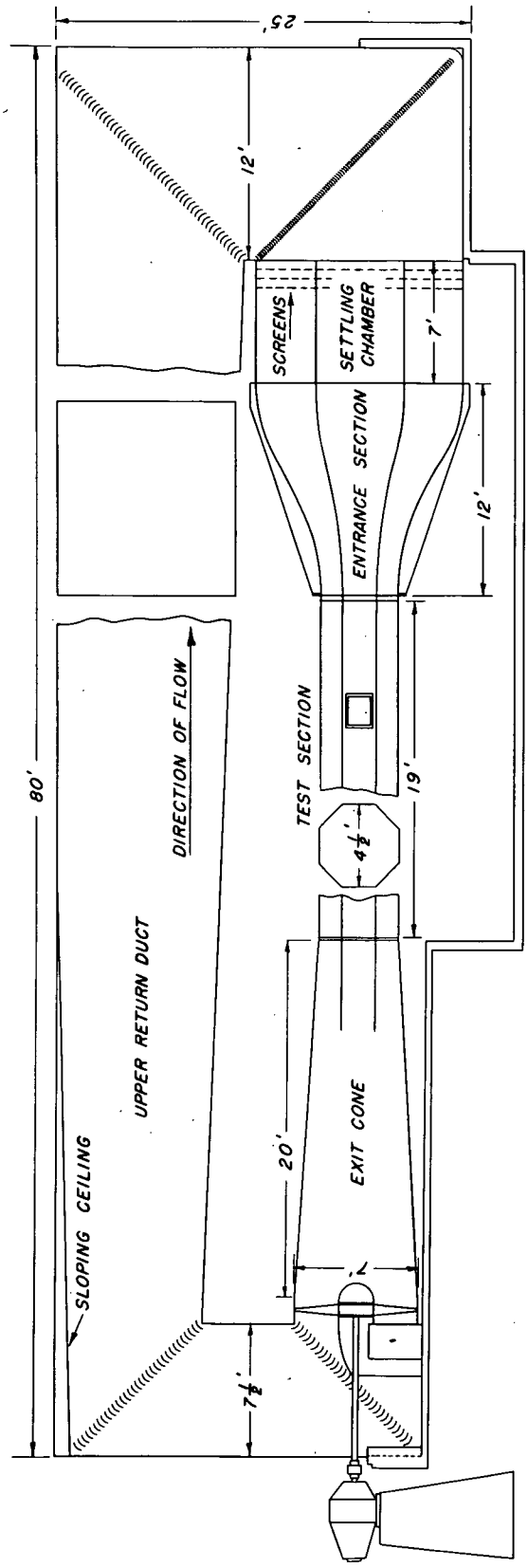

Figure 1.- Elevation view of $4\frac{1}{2}$- foot wind tunnel.

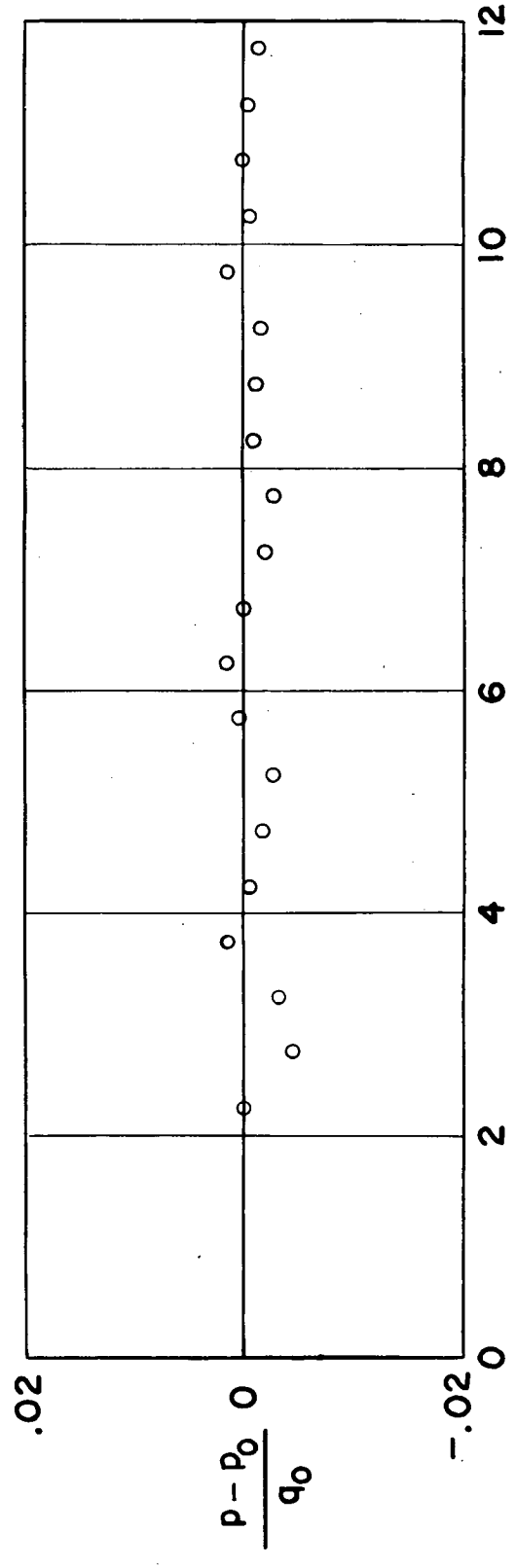

Figure 2.- Pressure distribution along flat plate.

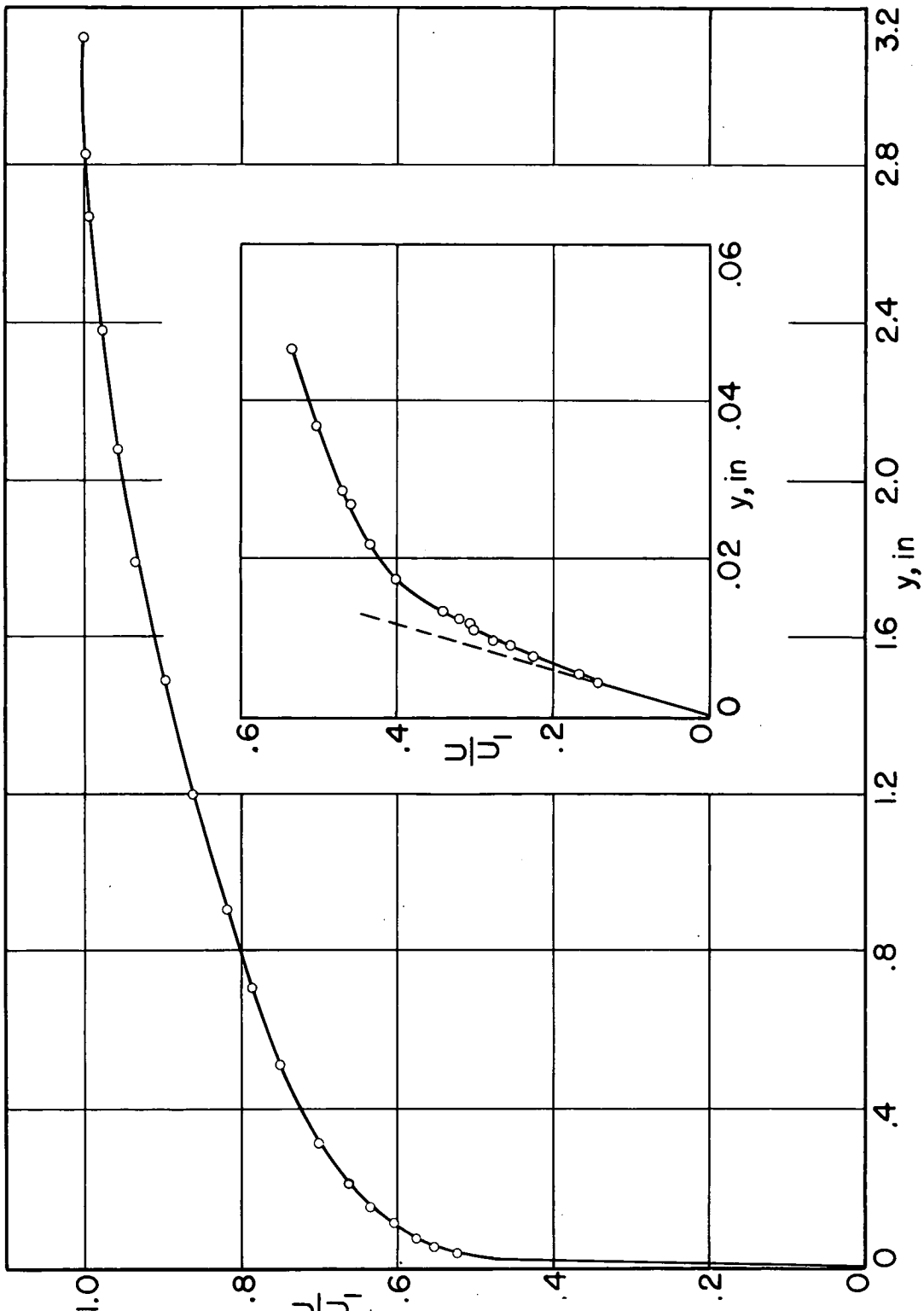

Figure 3.- Mean-velocity distribution.

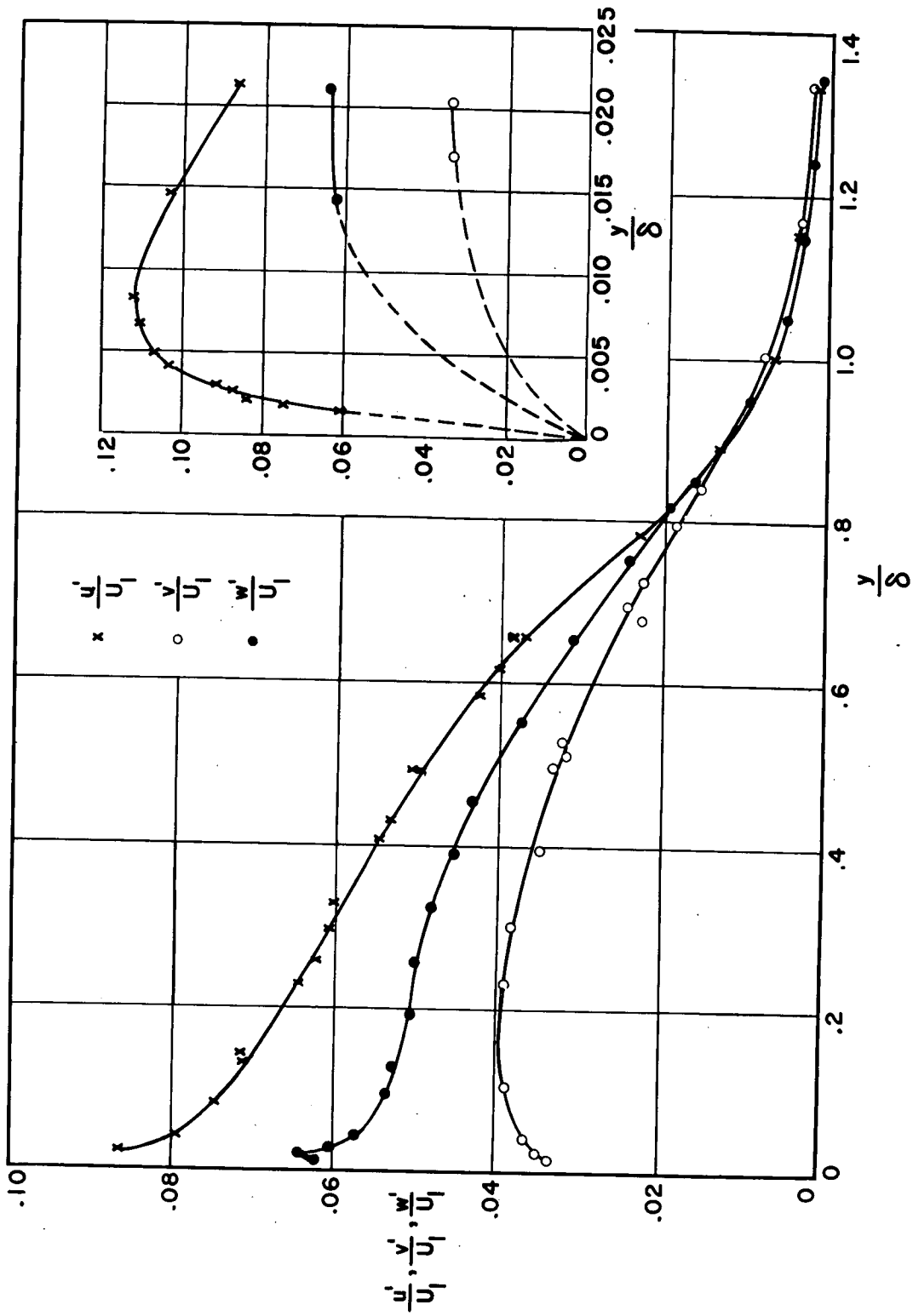

Figure 4.- Distribution of turbulence intensities.

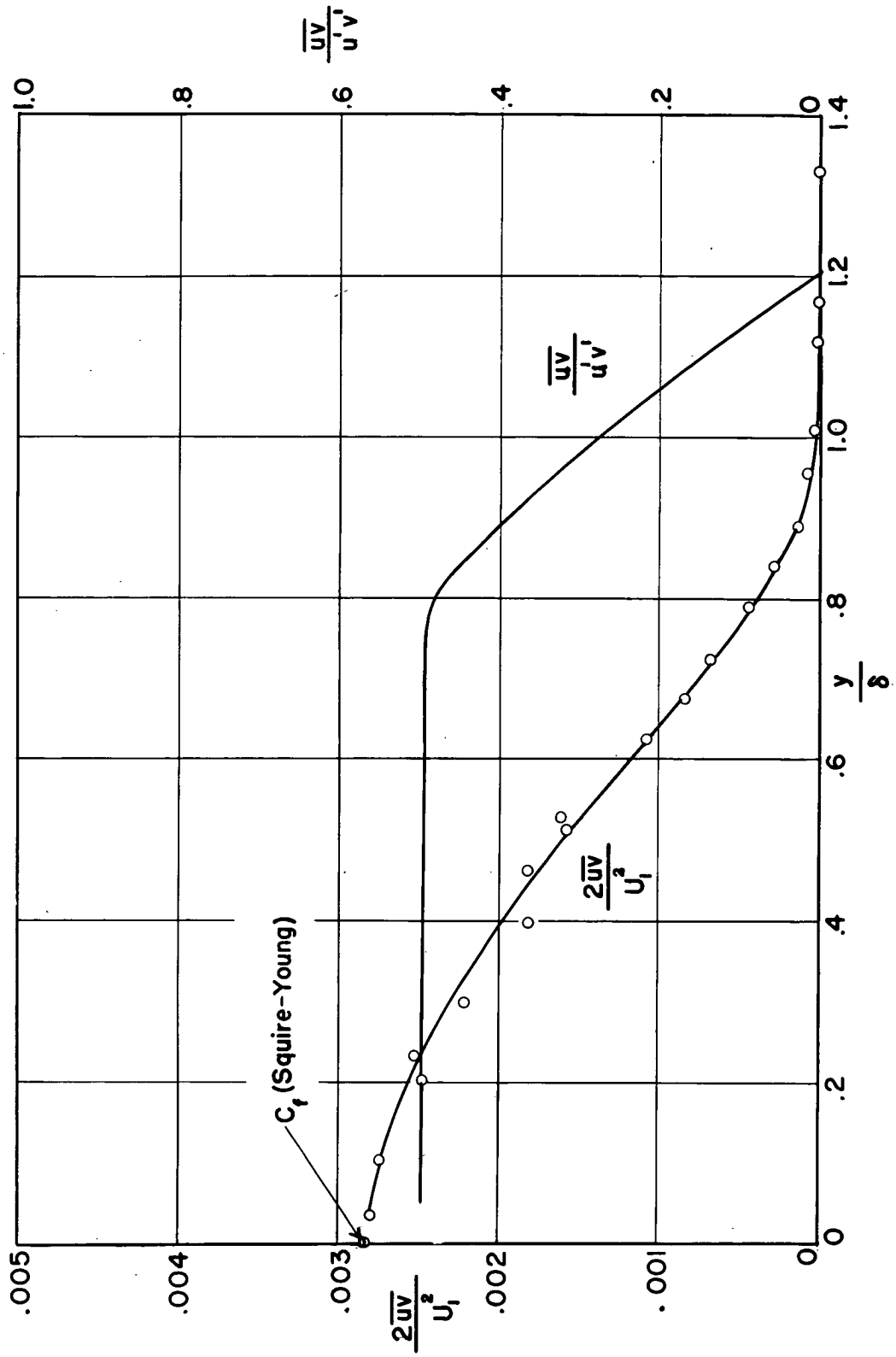

Figure 5.- Distribution of turbulent shearing stress and shear correlation coefficient.

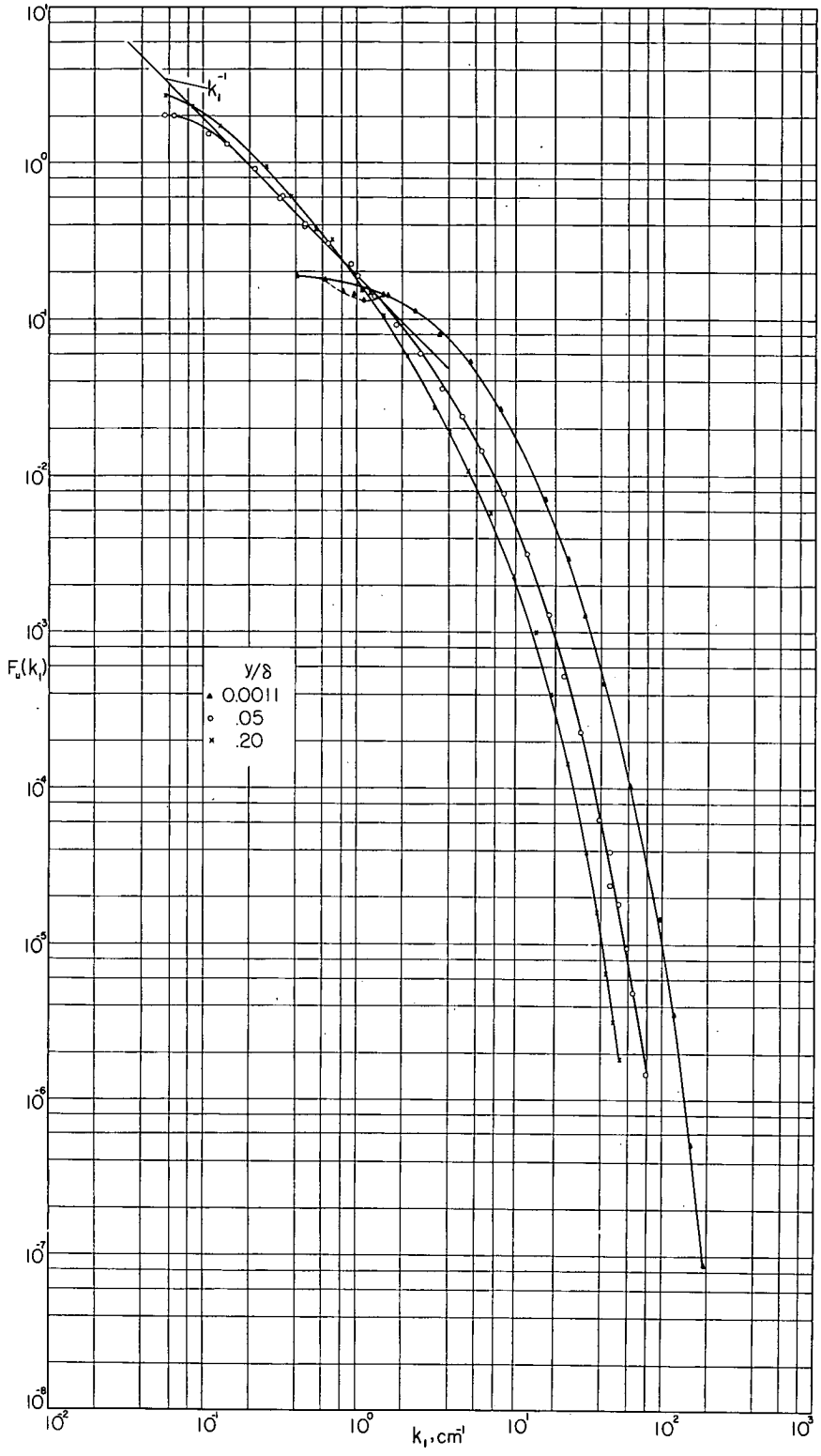

Figure 6.- Spectra of $\overline{u^2}$ in inner region of boundary layer.

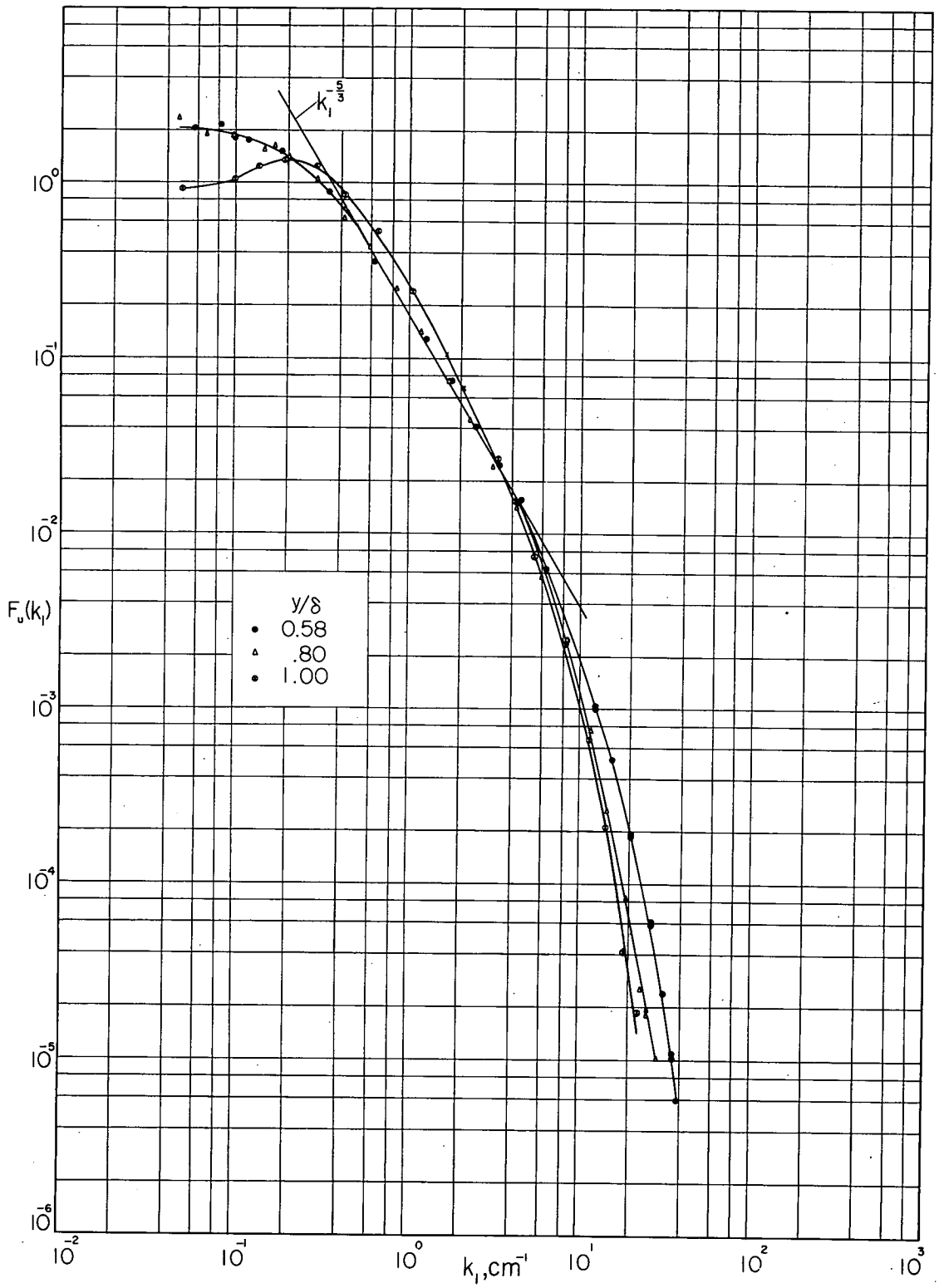

Figure 7.- Spectra of $\overline{u^2}$ in outer region of boundary layer.

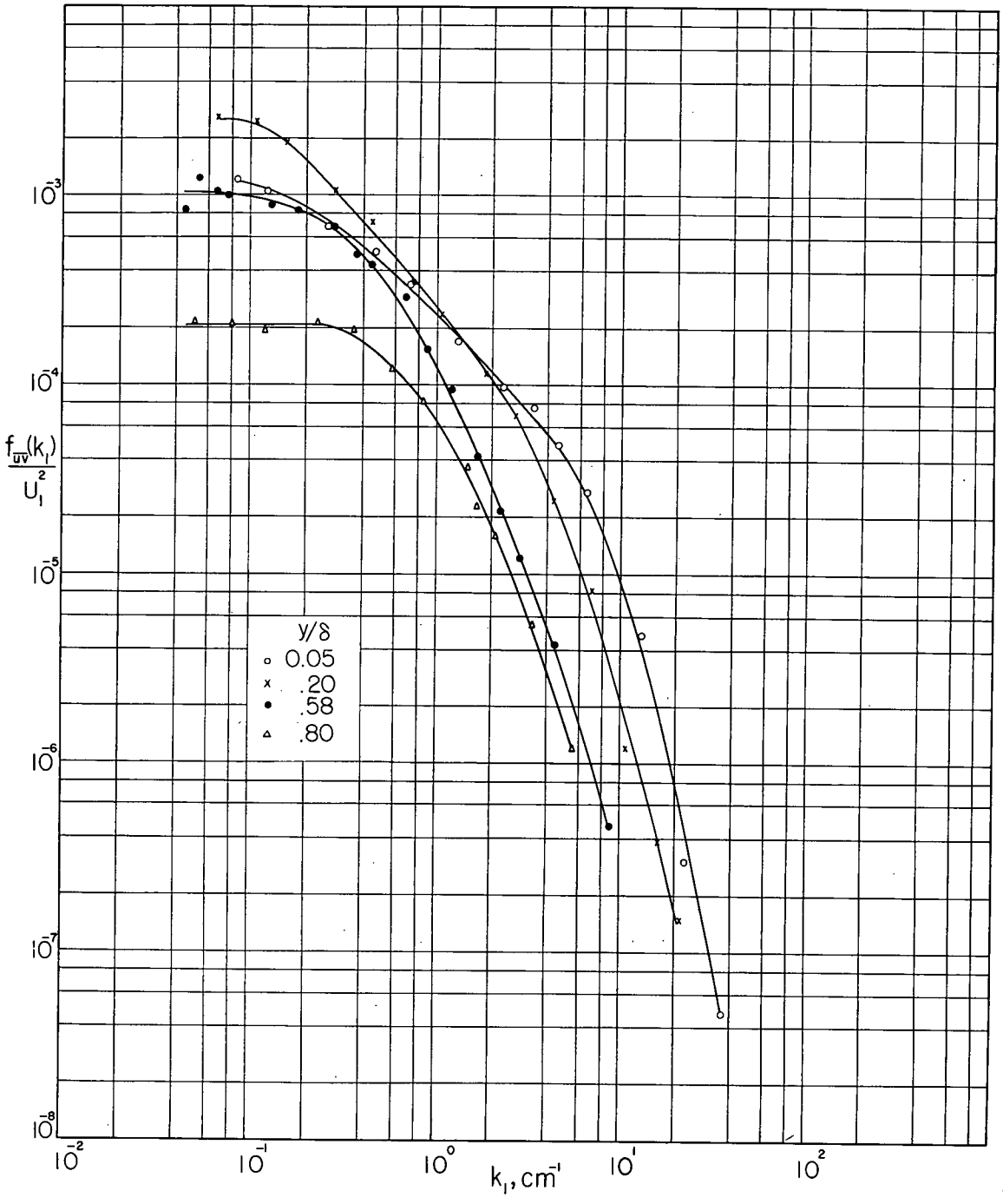

Figure 8.- Spectra of turbulent shear stress.

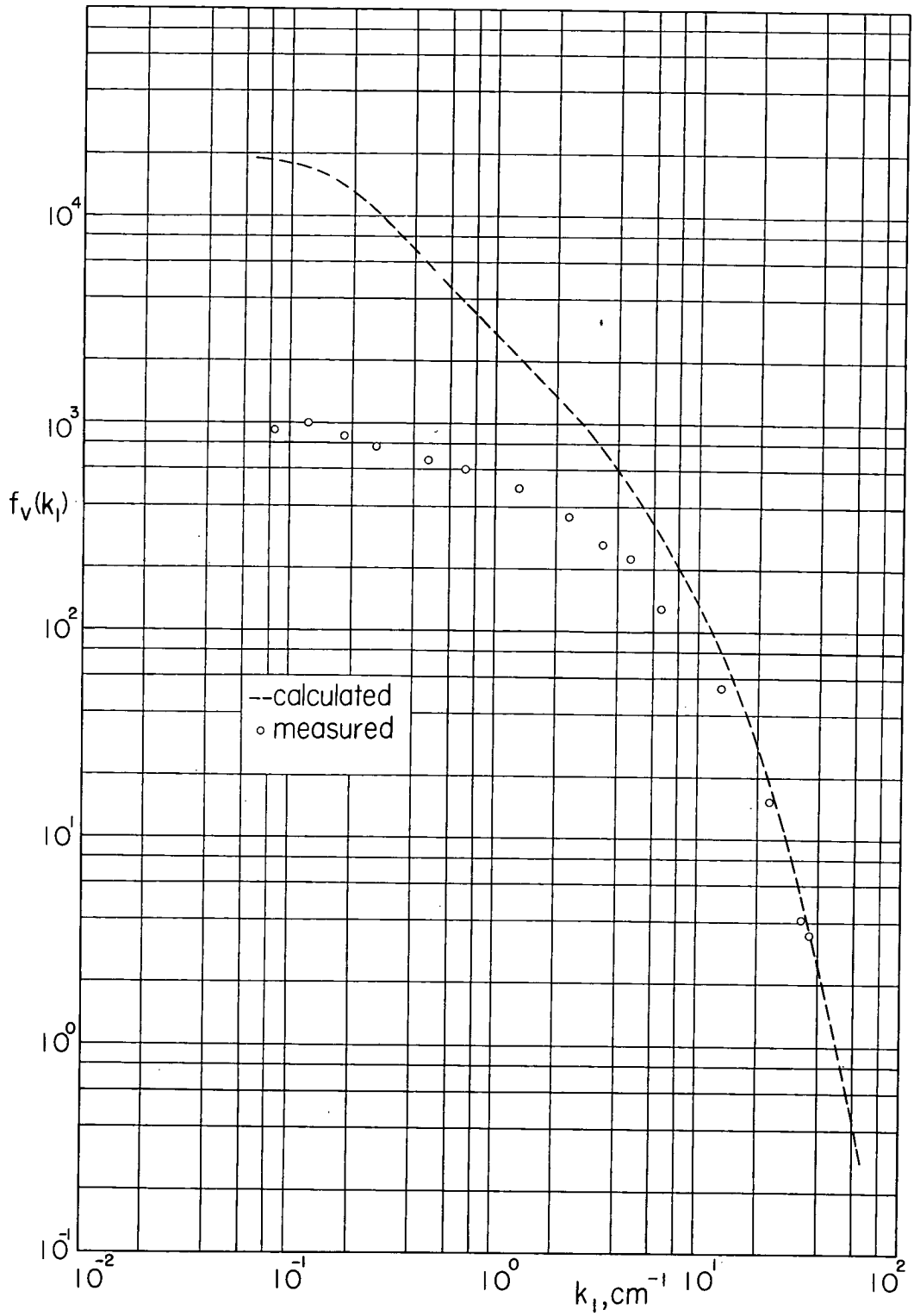

Figure 9.- Comparison of measured $\overline{v^2}$ spectrum with that calculated from measured $\overline{u^2}$ spectrum using isotropic relation; $y/\delta = 0.05$.

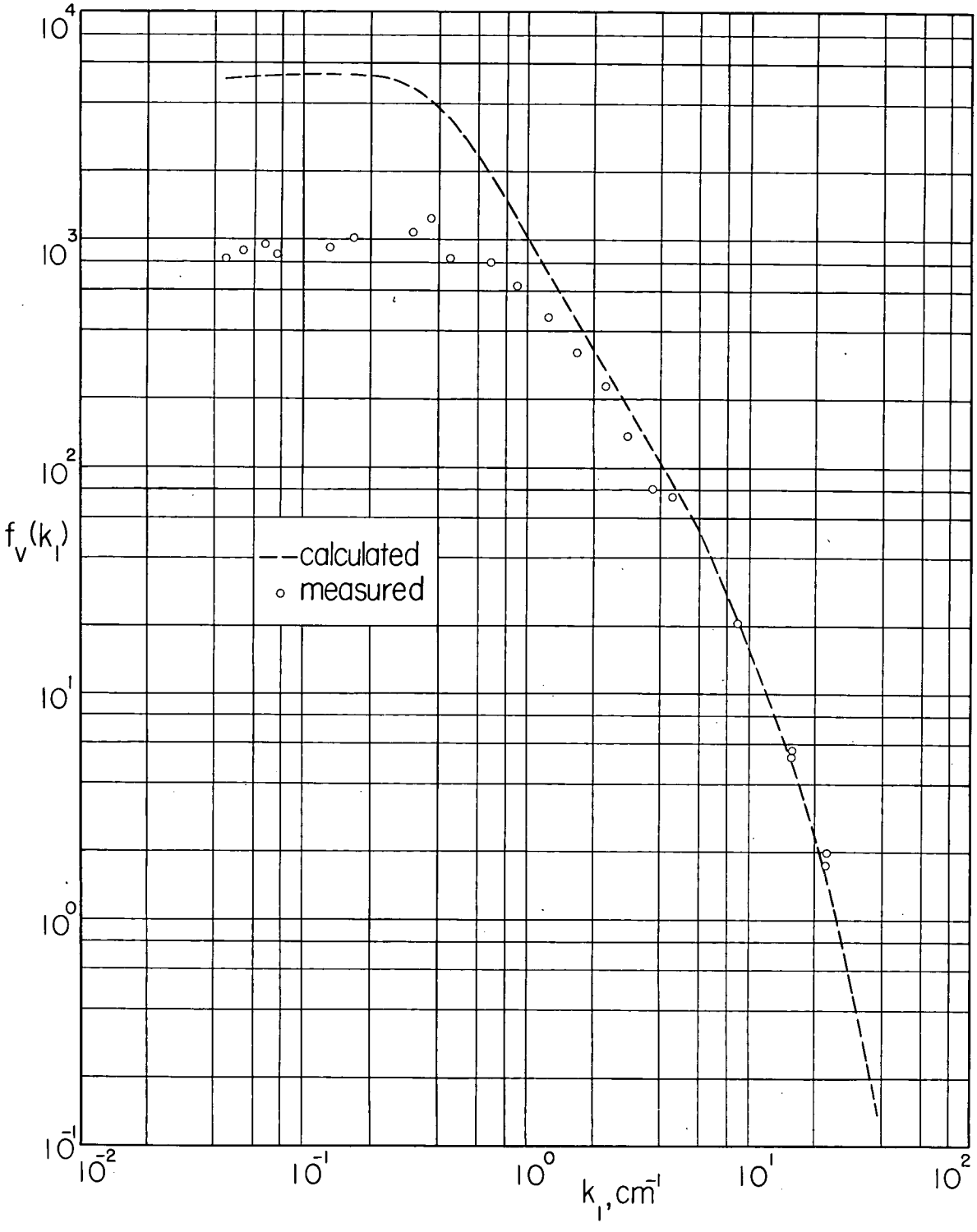

Figure 10.- Comparison of measured $\overline{v^2}$ spectrum with that calculated from $\overline{u^2}$ spectrum using isotropic relation; $y/\delta = 0.58$.

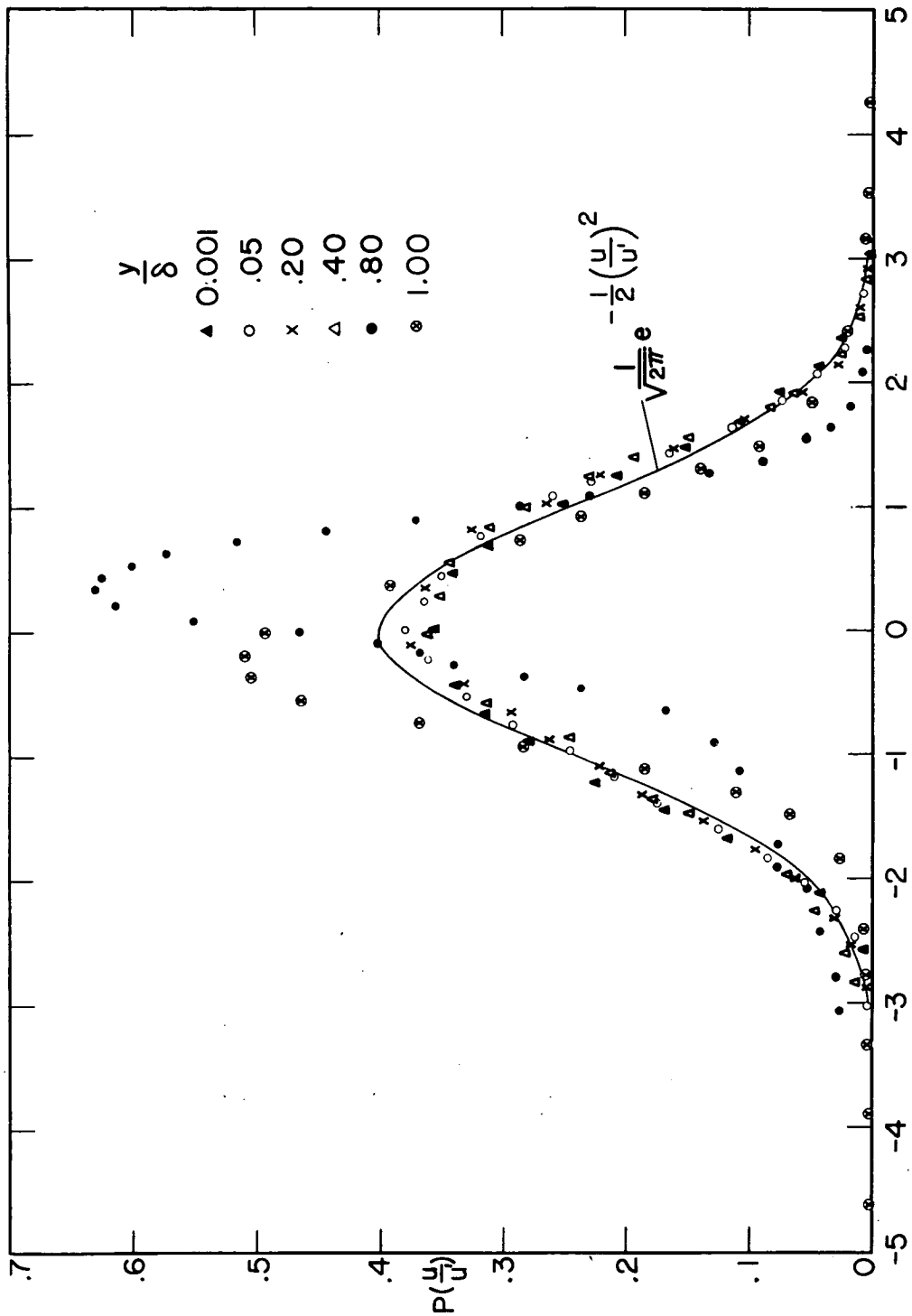

Figure 11.- Distributions of probability density.

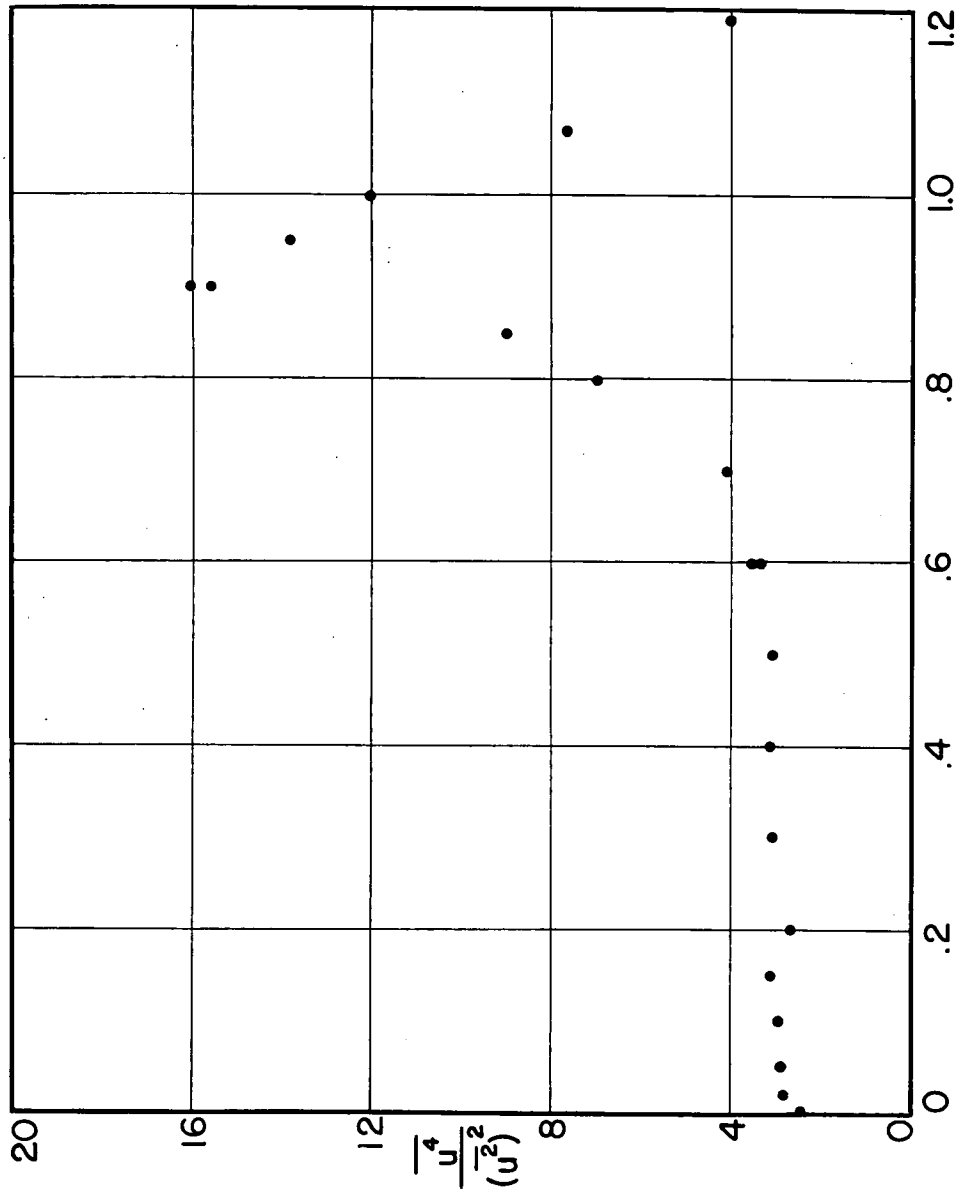

Figure 12.- Distribution of flattening factor.

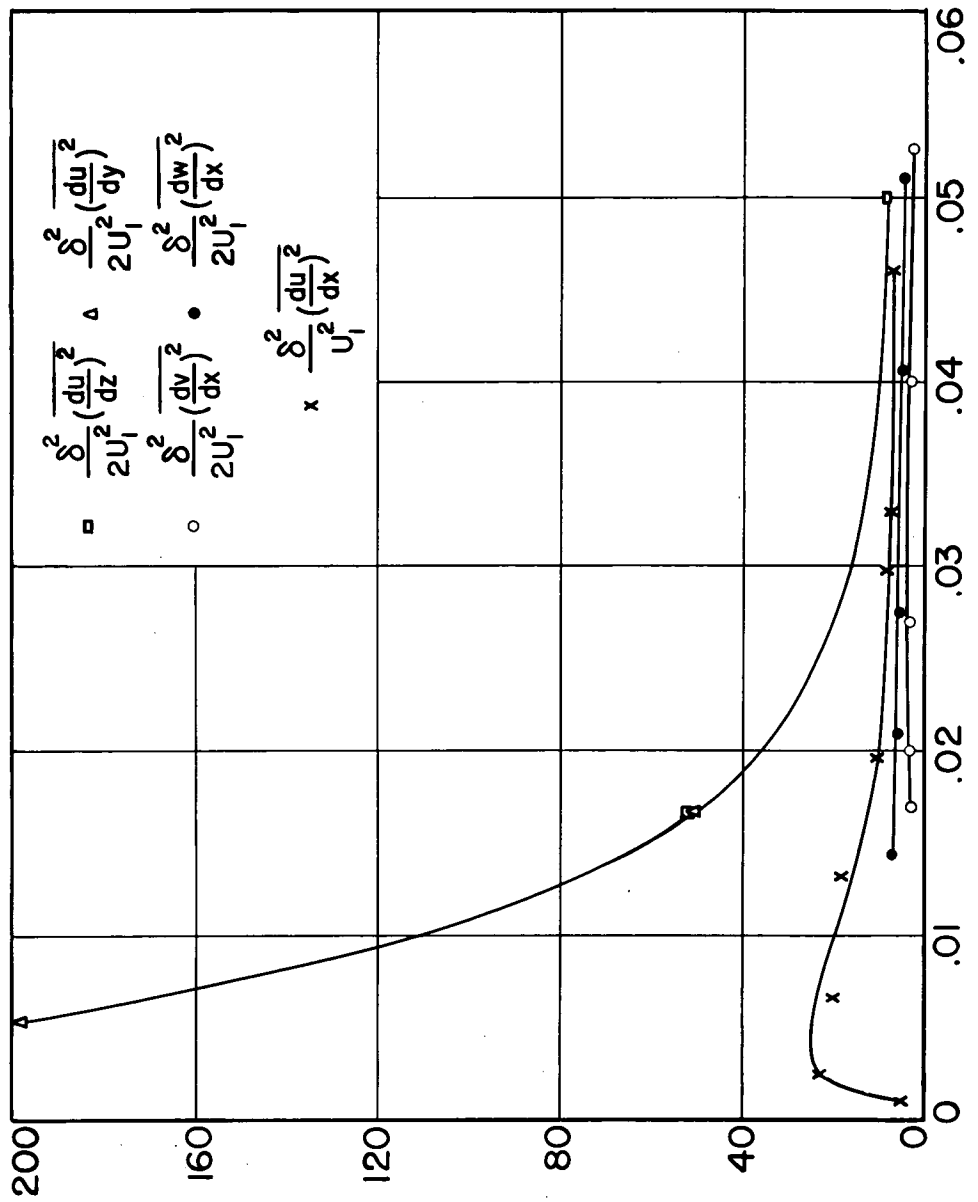

Figure 13.- Distribution of dissipation derivatives near wall.

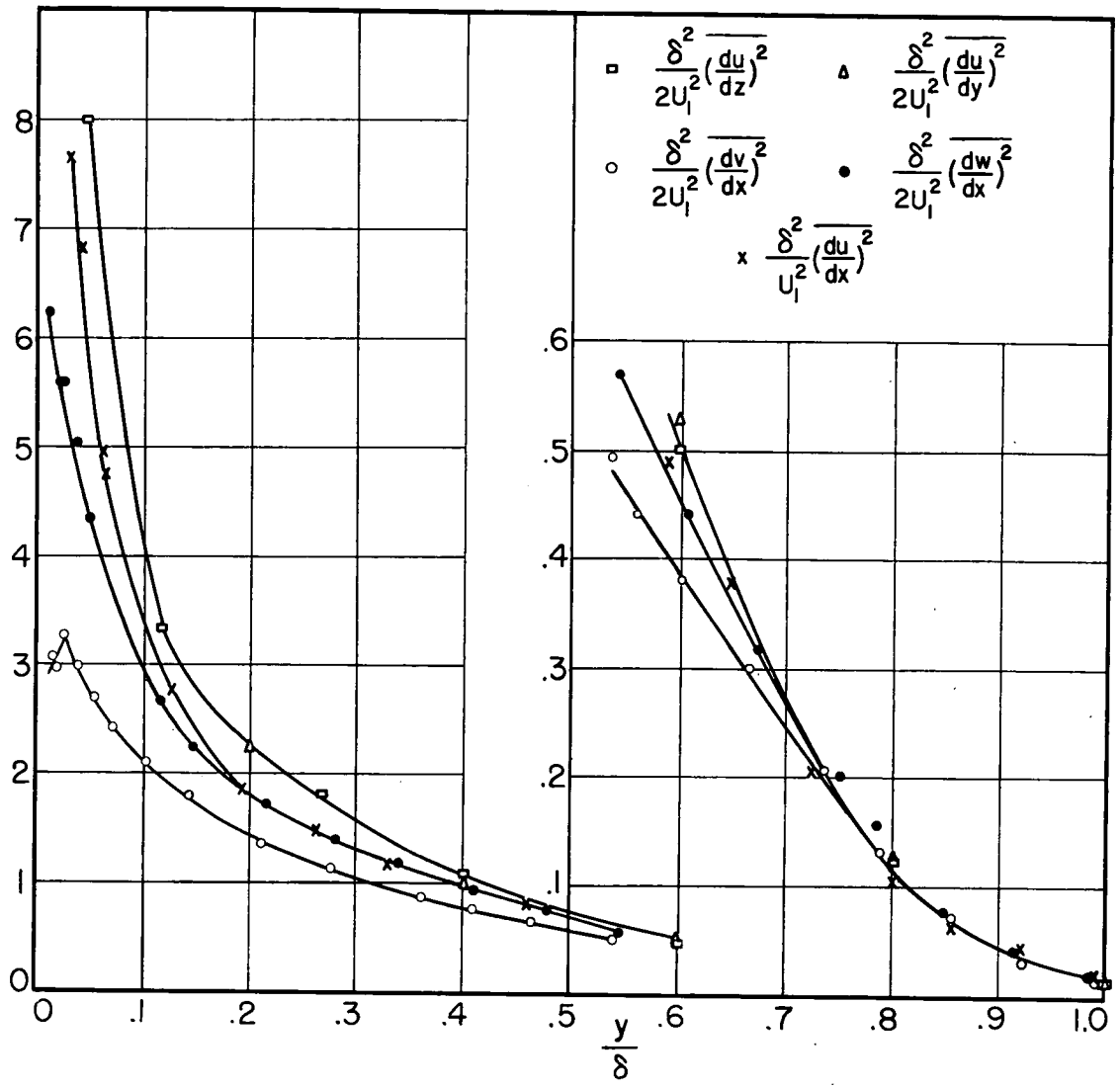

Figure 14.- Distribution of dissipation derivatives away from wall.

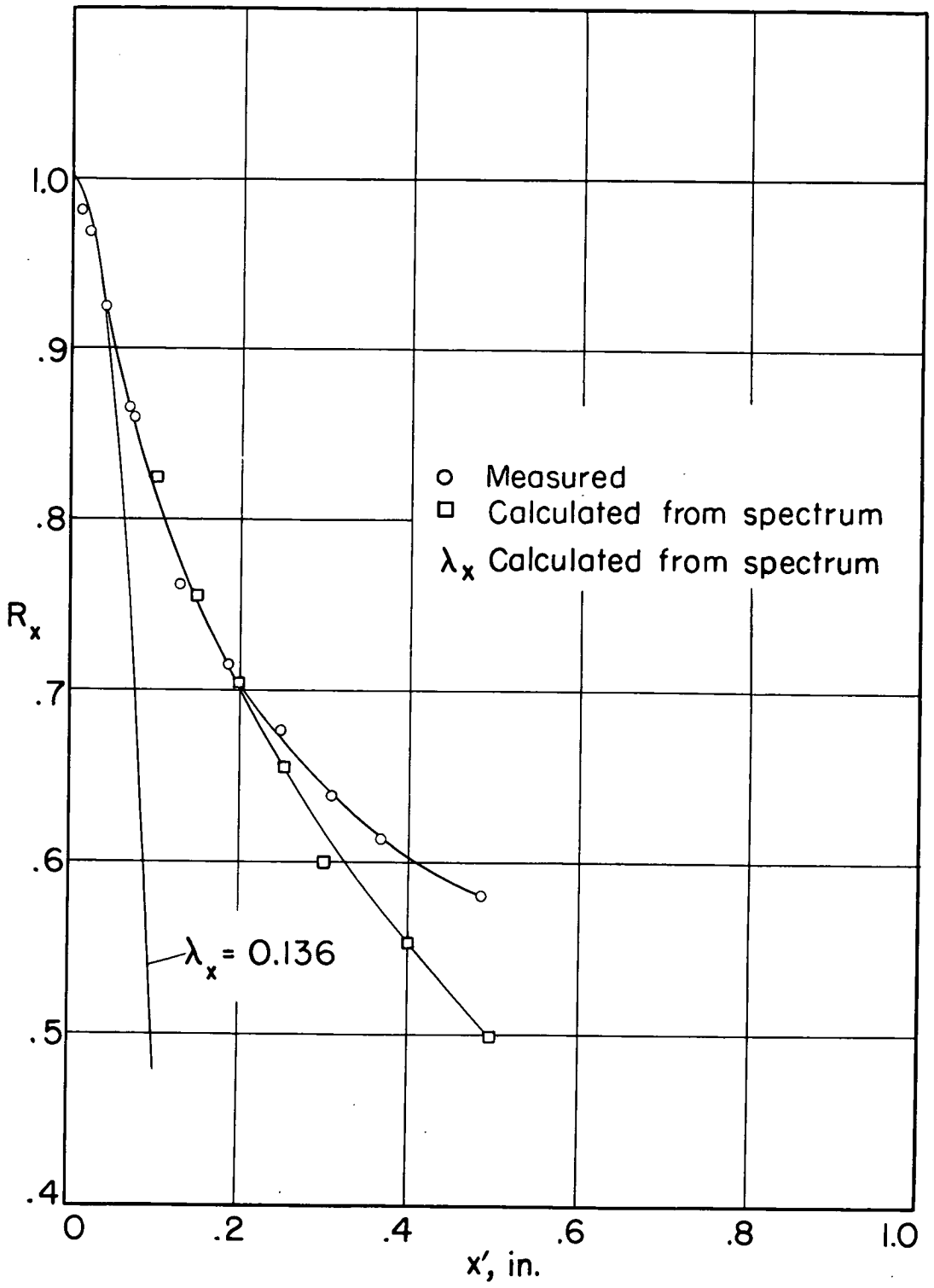

Figure 15.- Comparison of longitudinal correlation coefficient R_x obtained directly with that calculated from spectrum of $\overline{u^2}$; $y/\delta = 0.05$.

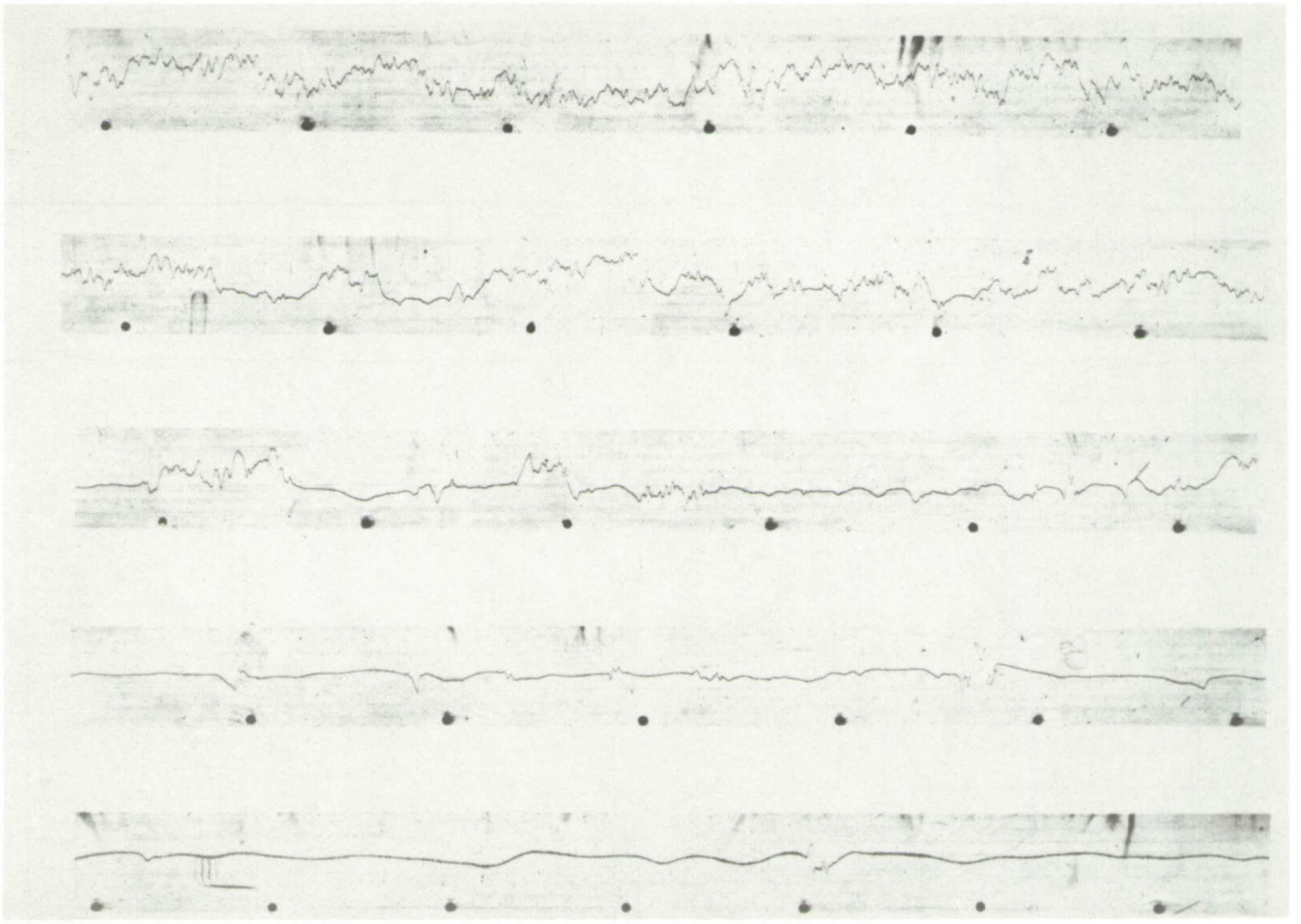

Figure 16.- Turbulence velocity u in boundary layer. U_1, 50 feet per second; timing dots, 60 per second.

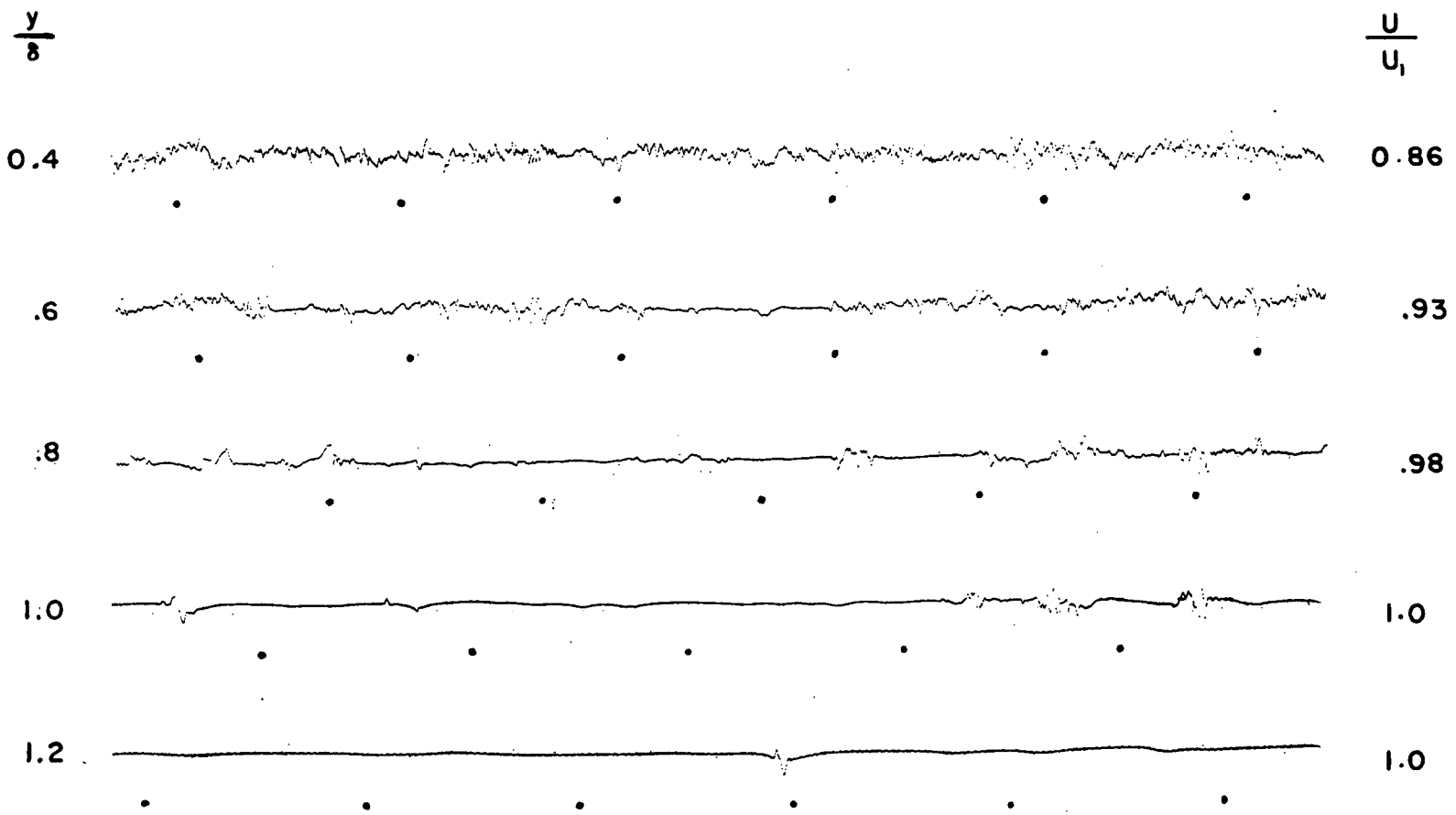

Figure 17.- Turbulence vorticity ω_x in boundary layer. U_1, 50 feet per second; timing dots, 60 per second.

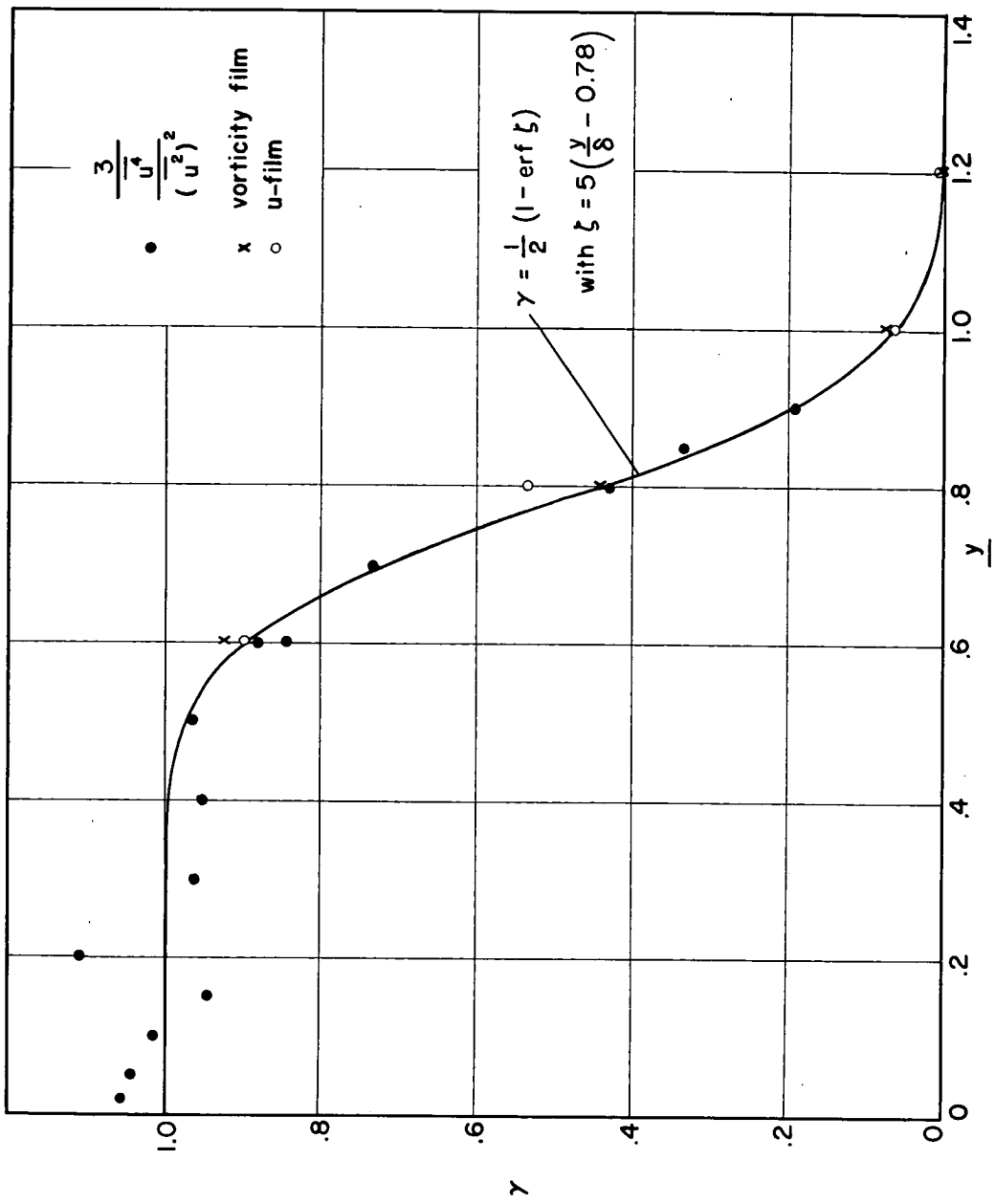

Figure 18.- Distribution of intermittency factor.

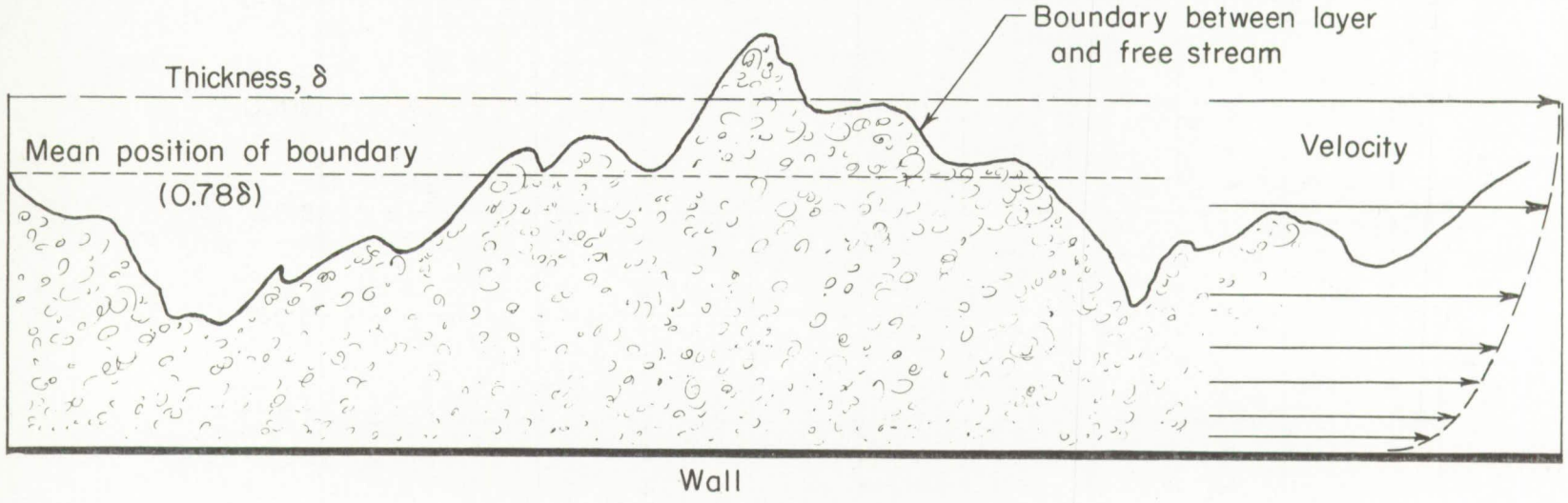

Figure 19.- Sketch of boundary layer.

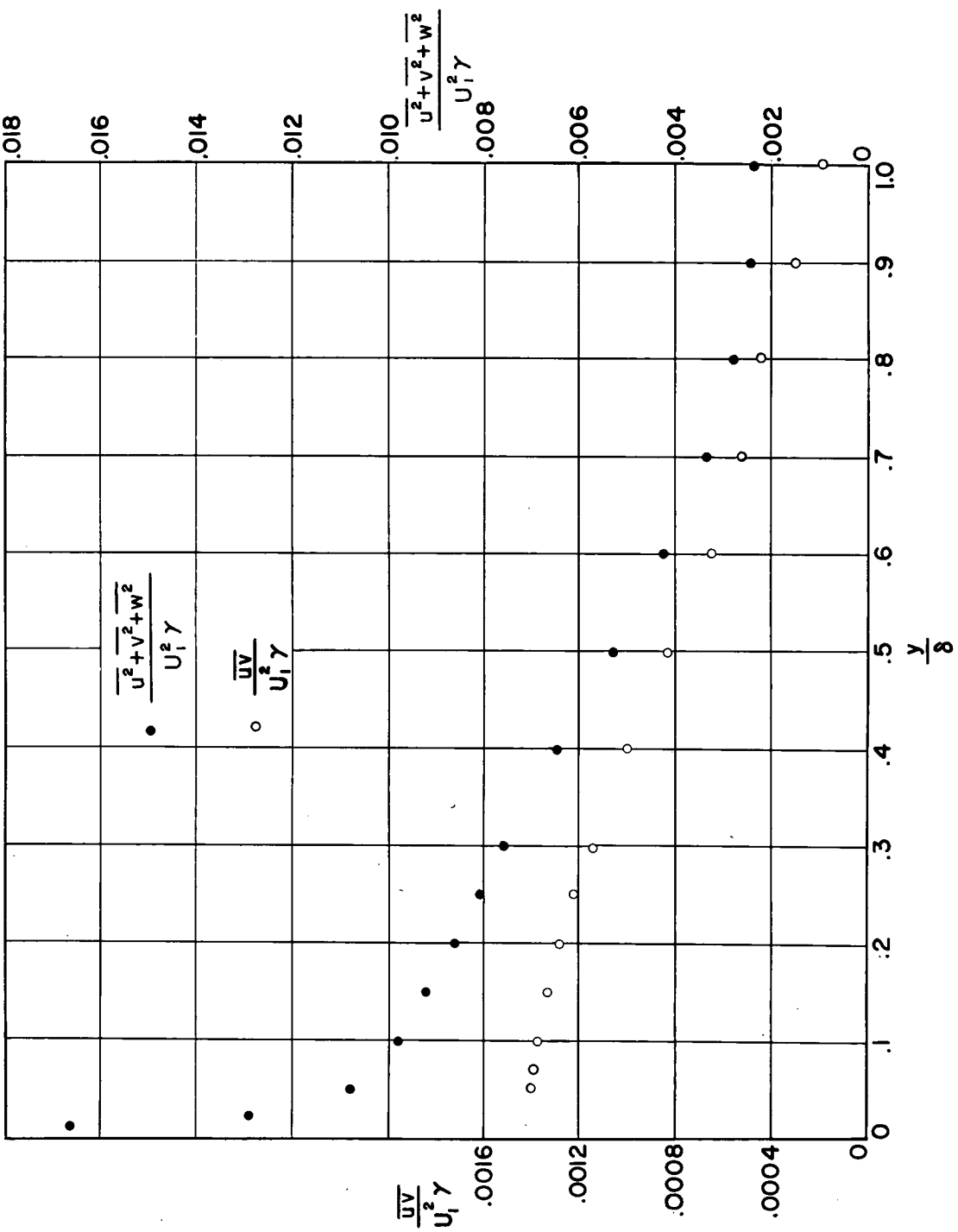

Figure 20.- Turbulent shear stress and turbulent energy divided by γ.

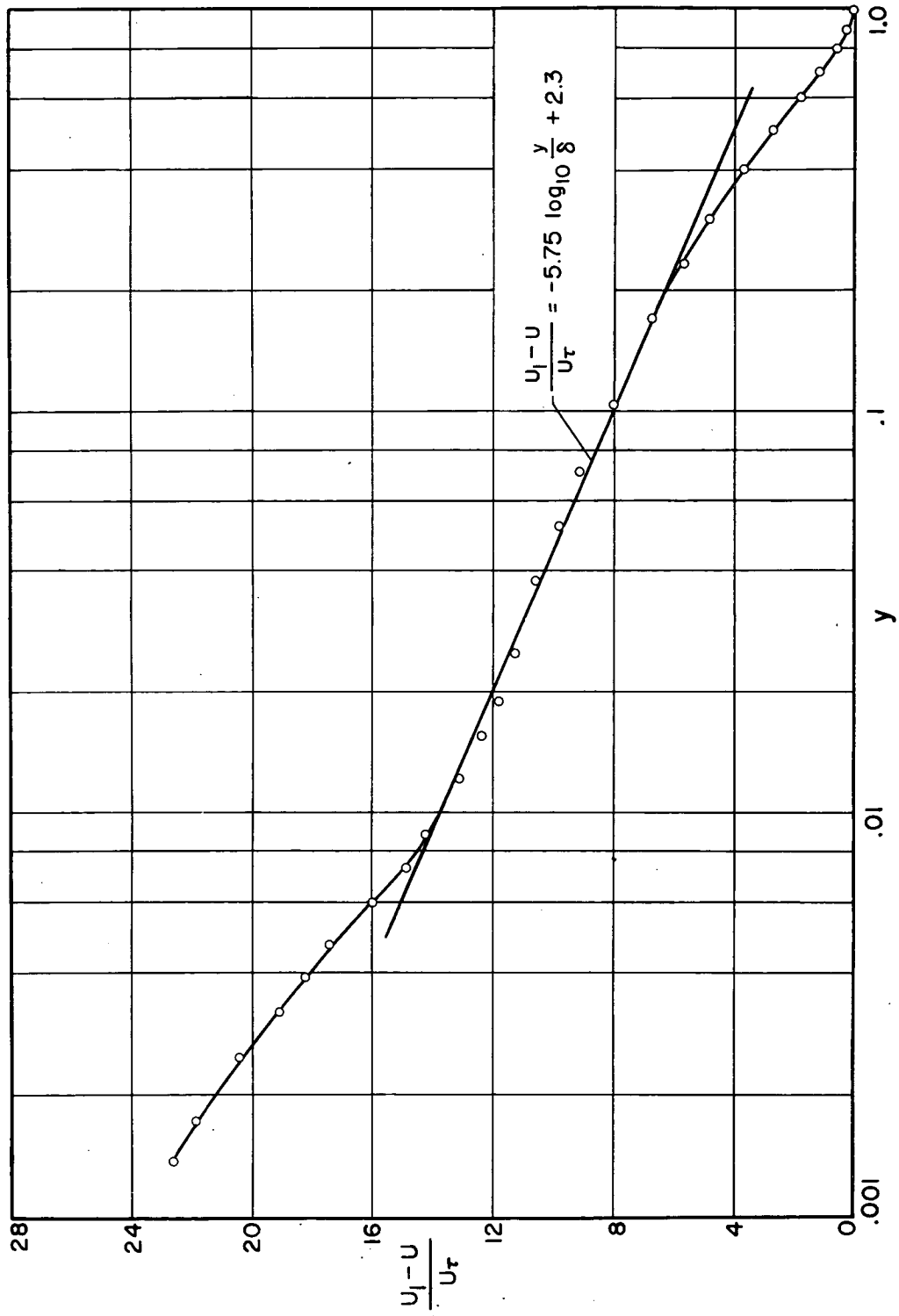

Figure 21.- Comparison of measured mean-velocity distribution with velocity-defect law.

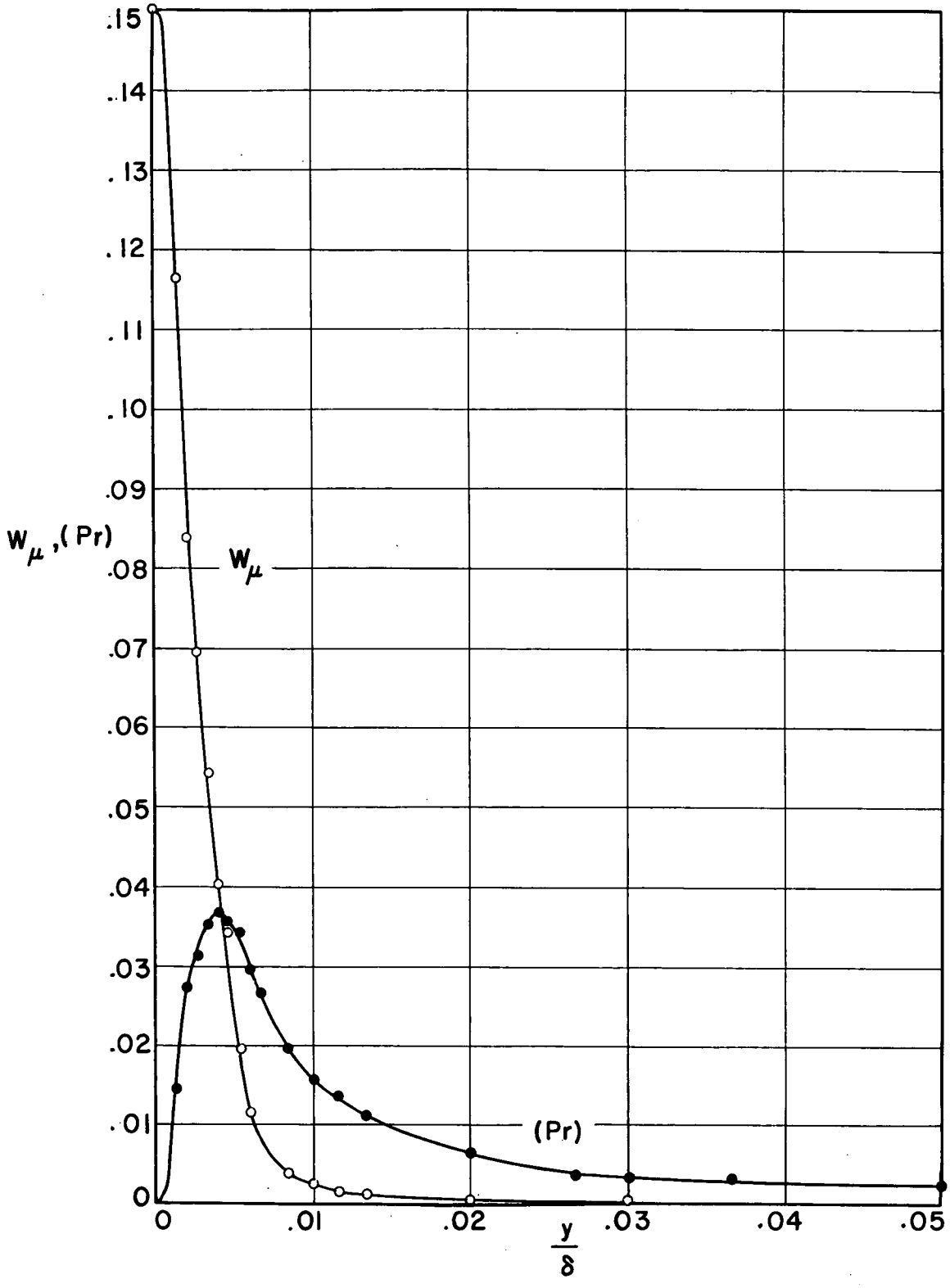

Figure 22.- Comparison of direct viscous dissipation with production of turbulent energy near wall.

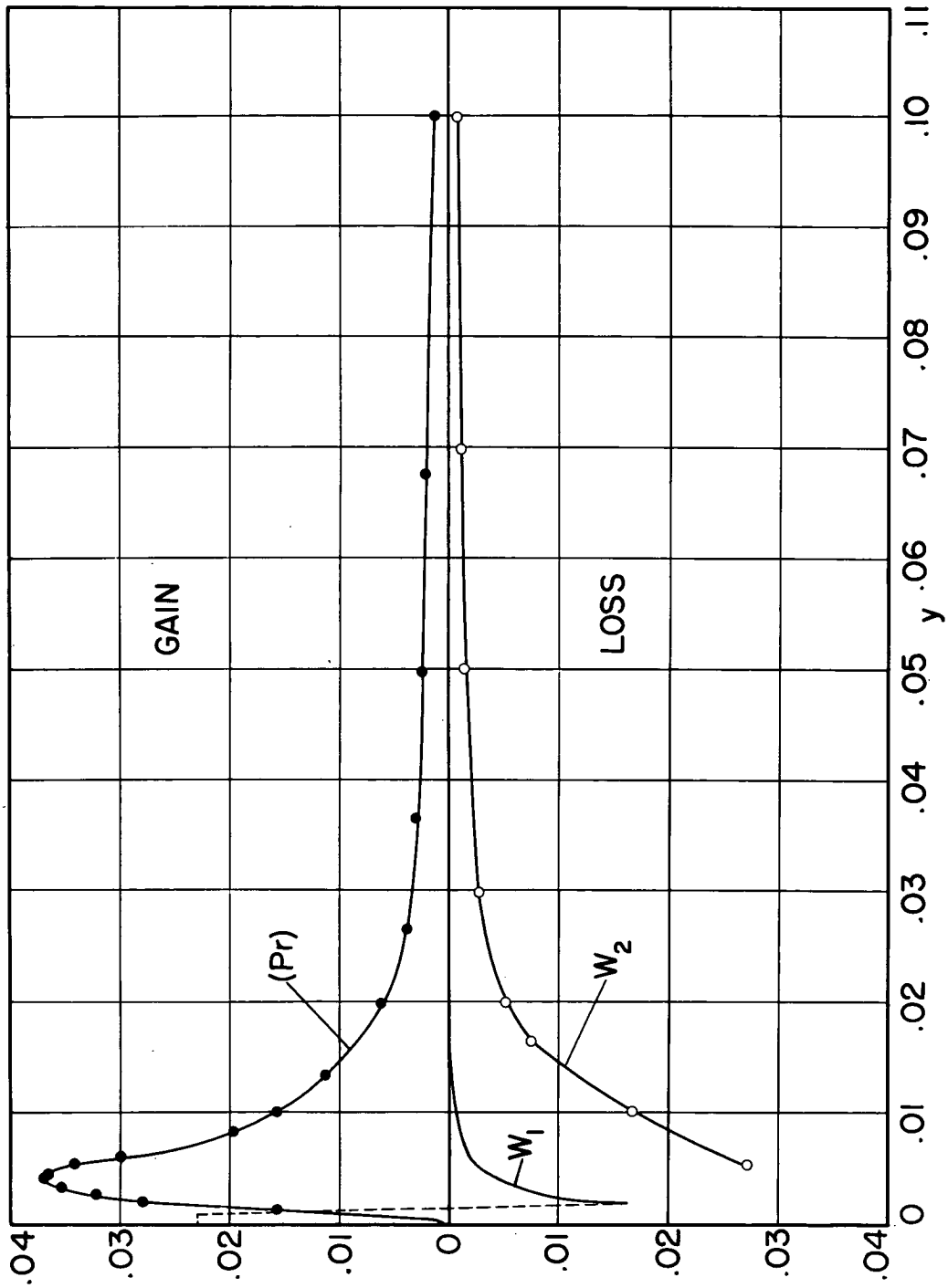

Figure 23.- Production and dissipation in region near wall.

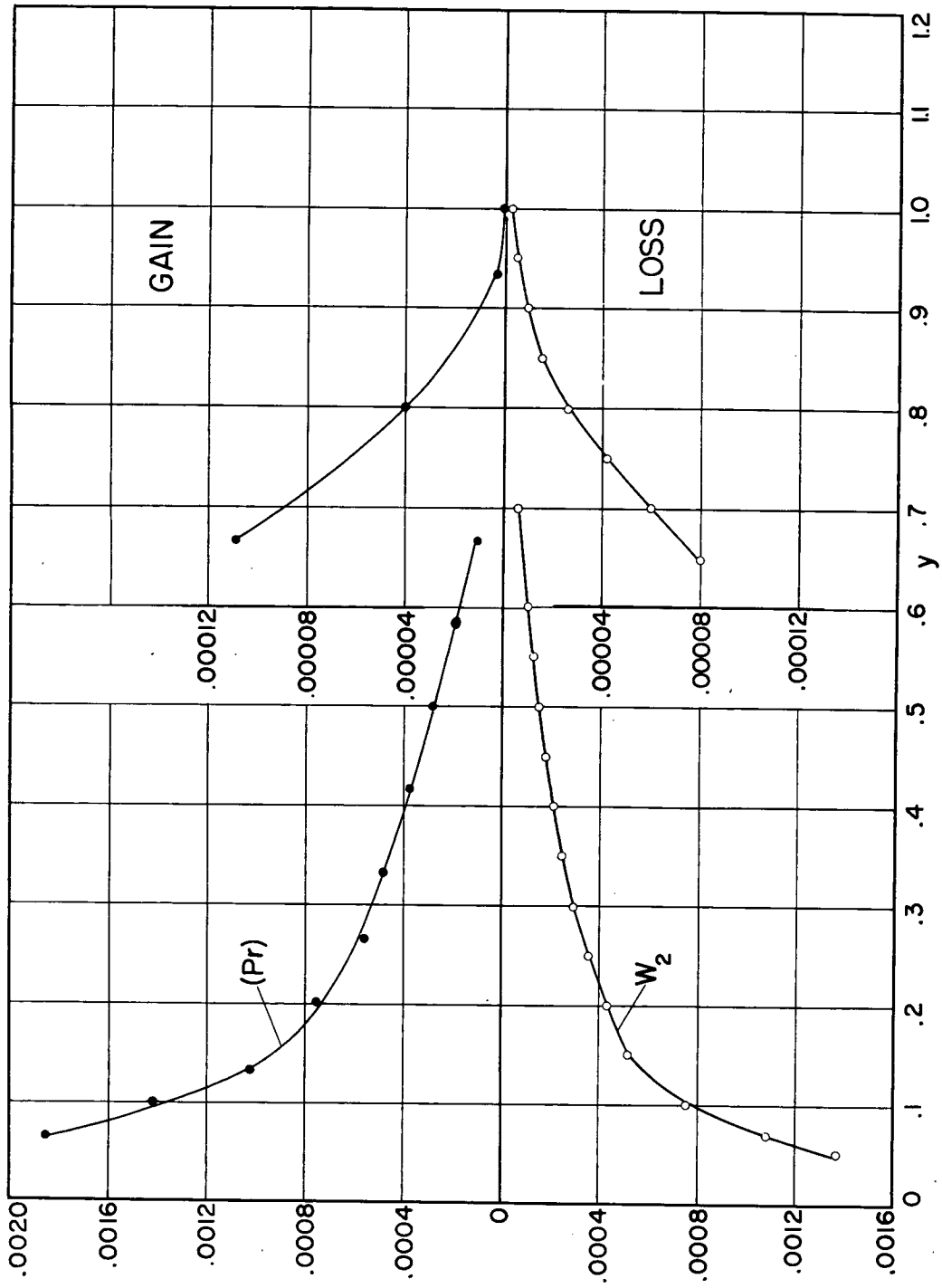

Figure 24.- Production and dissipation in region away from wall.

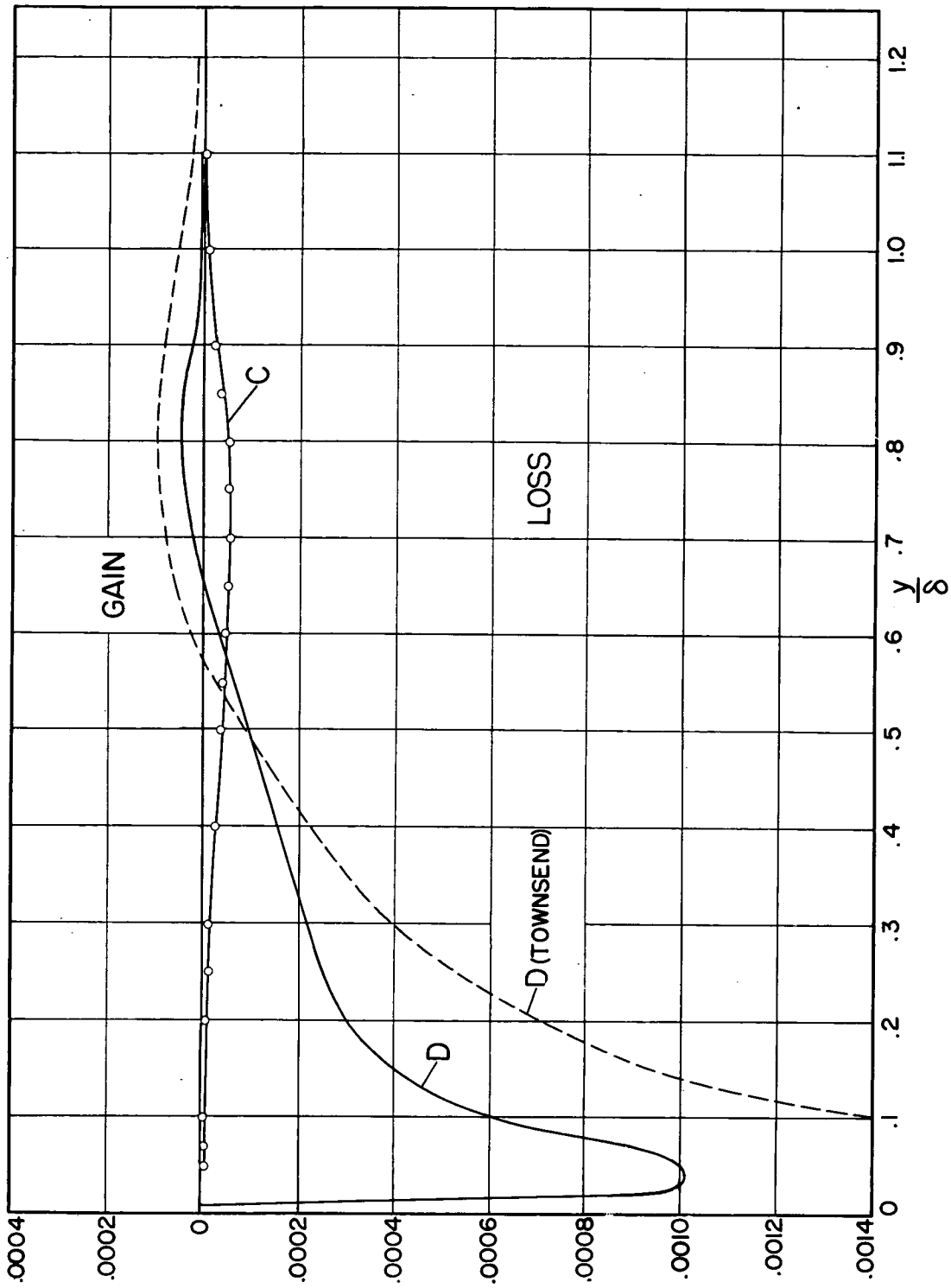

Figure 25.- Diffusion and convection.

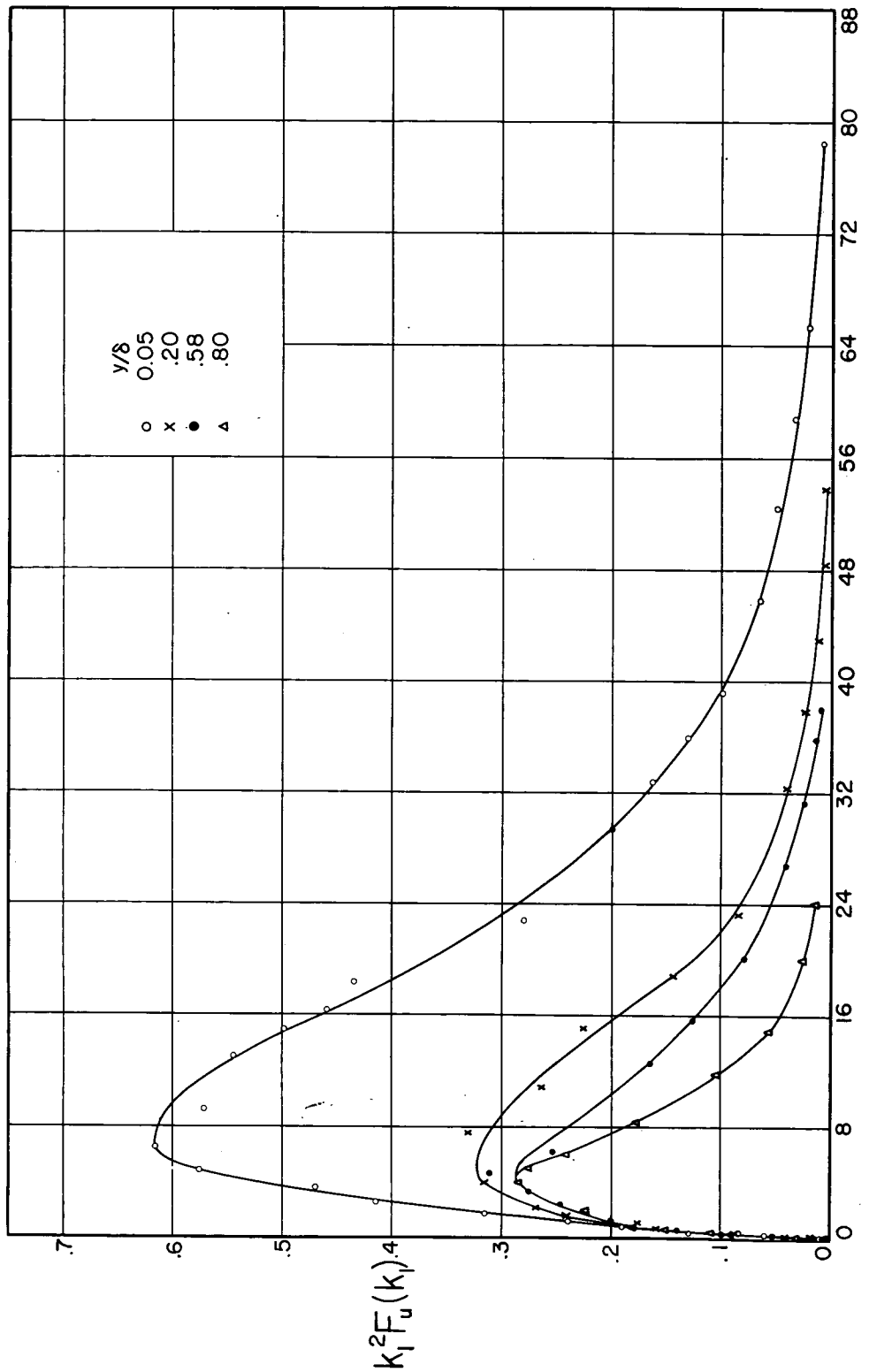

Figure 26.- Second moment of $\overline{u^2}$ spectra.